Signal Peptide of HIV-1 Envelope Functions to Modulate Glycosylation Impacting Exposure of V1V2 Epitopes

Chitra Upadhyay[1,2]*, Roya Feyznezhad[1], Liwei Cao[3], Kun-Wei Chan[4], Kevin Liu[1], Weiming Yang[3], Hui Zhang[3], Jason Yolitz[5], James Arthos[5], Arthur Nadas[6], Xiang-Peng Kong[4], Susan Zolla-Pazner[1], Catarina E. Hioe[1,2]

[1]Icahn School of Medicine at Mount Sinai, New York, NY, USA; [2]James J. Peters Veterans Affairs Medical Center, Research Service, Bronx, NY, USA, [3]Johns Hopkins University, Baltimore, MD USA, [4]Department of Biochemistry and Molecular Pharmacology New York University School of Medicine, New York, USA; [5]Laboratory of Immunoregulation, National Institute of Allergy and Infectious Diseases, National Institutes of Health, Bethesda, MD USA; [6]Institute of Environmental Medicine, New York University School of Medicine, New York, New York, USA

*Corresponding Author

Abstract

HIV-1 envelope (Env) is a trimer of gp120-gp41 heterodimers, synthesized from a precursor gp160 that contains an ER signal peptide (SP) at its amino-terminus. Each trimer is swathed by ~90 N-linked glycans, comprising complex-type and oligomannose-type glycans, that play an important role in evasion of neutralization by antibodies. Here, we demonstrate that HIV-1 Env SP can impact the glycan processing at multiple N-linked glycosites, including the N156 and N160 located in V1V2 on the trimer apex. Env expressed with SP from heterologous HIV-1 isolates display altered exposure of V2i, V2p and V2q epitopes impacting Env antigenicity and virus neutralization by antibodies targeting distinct V1V2 configurations. These results reveal the importance of HIV-1 SP in partly shaping the Env glycan profile. Thus, SP should be cautiously selected in designing the Env-based vaccines.

Keywords

HIV, HIV envelope, signal peptide, glycosylation, neutralization, V1V2 antibodies, trimer apex

Introduction:

HIV-1 envelope (Env) is the only viral antigen exposed on the surfaces of virions and infected cells. Env is synthesized as a precursor gp160 glycoprotein, which is targeted to the endoplasmic reticulum (ER) by the signal peptide (SP; signal or leader sequence) present at the amino terminus of the nascent protein. Generally SPs contain ~16-30 amino acids with a characteristic tripartite structure: a hydrophilic positively charged n-region, a central hydrophobic h-region, and a slightly polar carboxy terminal c-region with a cleavage site for signal peptidase (1). SPs are typically cleaved from the maturing protein co-translationally, but the ~30 amino-acid long SP of HIV-1 Env is cleaved post-translationally (2-5). This delayed SP cleavage is conserved across HIV-1 subtypes and functions as a quality-control checkpoint, ensuring proper folding and post-translational modifications of gp160 before its egress from the ER (6).

Within the ER, gp160 is decorated with ~30 N-linked glycans and undergoes folding and extensive isomerization until near native conformation is reached with the SP still attached. The SP is cleaved before gp160 reaches the Golgi for further glycosylation maturation and other post-translational modifications (2, 4, 7). In the Golgi, gp160 is cleaved by cellular furin to generate non-covalently linked gp120-gp41 heterodimers, three of which assemble to form the functional Env spikes. The apex of the trimer is made of three V1V2 domains from the gp120 protomers (8-10), which partially conceal the V3 loops underneath in the native “closed” conformation. High levels of antibodies against V1V2 and V3 correlated with reduced risk of HIV-1 acquisition in the RV144 Thai vaccine trial, the only trial demonstrating some efficacy thus far (11-13). While V1V2 and V3 contain immunogenic epitopes targeted by cross-reactive antibodies, these regions are

structurally dynamic and the epitopes are conformationally masked in most HIV-1 isolates (14). Dense glycosylation further shields V1V2, V3 and other epitopes (15-17). Nonetheless, some glycans also serve as components of epitopes for broadly neutralizing antibodies (bnAbs) (18-21).

Each V1V2 domain can form a 5-strand beta-barrel module, with the polymorphic V2 C-strand adopting α-helical or β-sheet conformations (22). Three types of V1V2 epitopes have been defined: V2p, V2i and V2q (23). The V2p type constitutes the α-helical peptide epitopes in the V2 C-strand that are recognized by monoclonal antibodies (mAbs) CH58 and CH59 from RV144 vaccinees (24) and the CAP228 mAb series from a virus-infected donor in South Africa (25). The V2i-type epitopes are made of conformational discontinuous segments in V1V2, some of which are near the integrin α4β7-binding motif (26, 27); these epitopes are recognized by mAbs such as 830A, 697-30D, and 2158 from infected US patients (26). The V2q type is comprised of quaternary neutralizing epitopes targeted by bNAbs, including the PG9 and PG16 (28). The V2q epitopes requires that the V2 C-strand assume a beta-sheet structure (19). The V2q epitopes also include glycans at positions N156 or N173 and N160 on the V1V2 apex (19, 29), which, with N197 and N276 glycans creates the conserved ‘trimer-associated mannose patch’ (TAMP). Other Abs such as mannose-binding 2G12 and some PGT bnAbs (e.g. PGT121, PGT128, PGT135) also directly target glycans at N295, N332, and N392 (30-32), which form the intrinsic mannose patch (IMP) (33). The V2i epitopes, in contrast, do not include glycans, but are conformationally dependent on proper V1V2 glycosylation and folding, and require the presence in the V2 C-strand of a beta-strand configuration (22, 23). Moreover, the propensity of V2 C-strand to adopt α-helical and β-sheet structures recognized by V2p

and V2q mAbs, respectively, is influenced by glycosylation (23). Thus, changes in glycosylation can impact HIV-1 interaction with Abs against V1V2. This would be expected to be true for other Env regions as well.

HIV-1 Env glycosylation is dictated in part by the SP (34, 35). The SP displays remarkable sequence diversity (34, 36, 37), the reason for which is not fully understood; nonetheless, the native Env SP has been replaced by unrelated SPs (e.g. SPs of CD5 and tissue plasminogen activator (tPA)) to promote the secretion of soluble Env (5, 37-39). Likewise, the herpes simplex virus (HSV) SP was used to express the gp120 tested in RV144 clinical trial (40-42). Beyond protein targeting, SP also influences protein folding, modification, localization, and topology (3, 43-45). Mutations in SPs are suggested to impair transport and alter maturation as a result of incomplete glycosylation in the ER and Golgi, leading to several human diseases (46). For example, a mutation in the hydrophobic core of the SP of preproparathyroid hormone is suggested to impact its translocation across the ER to cause a functional defect associated with familial isolated hypoparathyroidism (46). Mutations in the SP of TGF-beta type I receptor results in resistance to TGF-beta in B cell chronic lymphocytic leukemia patient (47). SP mutations also have been associated with other metabolic, developmental, cardiovascular, and autoimmune human diseases (47-51). In the case of HIV-1 Env, we have demonstrated that single point mutations in the SP of HIV-1 Env REJO and JRFL can alter HIV-1 Env glycosylation to affect virus neutralization and DC-SIGN mediated transmission (34, 52). The effect of SP mutations on other viruses has not been much studied, but the extremely long envelope SPs of retroviruses like foamy virus and mouse mammary tumor virus have been shown to mediate additional functions other than ER targeting. The cleaved SP

product from foamy virus is associated with cell-free virions and is critical for virus release from infected cells (53). The SP of the MMTV envelope precursor is reported to function as a nuclear export factor for intron-containing transcripts (54). Collectively, these studies highlight the significant role of SPs and their profound effects on the functions of associated proteins and viruses.

This study investigated SP sequence variations found naturally in HIV-1 isolates on the virus and Env phenotypes. Using three Env backbones and SPs from viruses representing different clades, neutralization tiers and clinical stages (Fig S1), we tested the impact of different SPs on the same Env backbones. Site-specific glycosylation analysis revealed Env expressed with SPs from different HIV-1 strains to have altered proportions of oligomannose and complex glycans at many glycosites including N156 and N160 on the V1V2 trimer apex. The modified glycan compositions were associated with perturbed virus neutralization and Env binding, especially by antibodies targeting V1V2. The study presents important, previously unknown, details about the critical contribution of HIV-1 Env SP that can have important implications for vaccine designs.

Results:

Glycosylation changes of SP-swapped vs WT Envs on CMU06 virions

To investigate the functional consequences of Env SP diversity, we selected SPs from isolates that display different neutralization sensitivity and represent different clades and clinical stages (37, 55, 56). The SP of CMU06 Env (CRF01_AE, tier 2, acute) was swapped with SPs from MW (clade C, tier 1A, chronic), 398F1 (clade A, tier 1A, acute), CH119 (CRF_07, tier 2, chronic) and 271.1 (clade C, tier 2, acute), while maintaining the SP cleavage site of the parental CMU06 (Fig 1A). All SP-swapped viruses were infectious and had comparable levels of Env incorporated into virions (Fig 1B and C), demonstrating that SP swapping had no deleterious effect on Env expression and virus infectivity.

To examine the effect of SP swapping on glycosylation, Envs from sucrose-pelleted WT vs SP-swapped CMU06 viruses were probed in Western blots with anti-gp120 mAbs and lectins that recognize distinct sugar moieties: GNA (terminal α1-3 and α1-6 mannose on high-mannose glycans) and AAL (α1-6 or α1-3 fucose on complex glycans) (57, 58). Upper and lower Env bands were detected by anti-gp120 mAbs and lectins. GNA binding to the upper bands of SP-swapped Envs was increased by ~2-fold vs WT, whereas binding to the lower bands were minimally altered (Fig 1D). Differences were also observed in AAL binding to the upper and lower bands of all SP-swapped Envs. These data demonstrated modulations in glycan contents of SP-swapped Envs vs WT that were modest but enriched for terminal α1-3 and α1-6 mannose-bearing oligomannose-type glycans and fucosylated complex glycans.

To further discern glycan alterations at specific glycosites, CMU06-WT, CMU06-398F1, and CMU06-271.1 were analyzed by LC-MS/MS upon Endo-H and PNGase digestion. Of 28 potential glycosites present on CMU06 Env (Fig S2), oligomannose glycans, complex glycans, and unoccupied glycosites were identified with coverage of 57% (16/28), 64% (18/28), and 54% (15/28) respectively. Hybrid-type glycans were indistinguishable from oligomannose-type, as both were digested by Endo-H. Noticeable alterations were found at many glycosites in both gp120 and gp41 of CMU06-398F1 and CMU06-271.1 vs CMU06-WT, (Fig 1E and 1F). Of the 12 glycosites detected on gp120, the percentage of oligomannose glycans was same on CMU06-WT (41%) and CMU06-271.1 (41%) but changed to 47% on CMU06-398F1. Of the three gp41 glycans, complex types were predominant on WT (74%) and the amounts were altered to 88% on 398F1 and 41% on 271.1. Consistent with GNA data (Fig 1D), LC-MS/MS data demonstrated an increase in total oligomannose glycans of CMU06-398F1 (39%) and CMU06-271.1 (43%) vs CMU06-WT (38%). The data also showed alterations in the total complex glycans (47%: 398F1 and 38%: 271.1 vs 51%: WT), but LC-MS/MS could not delineate the specific proportion of fucose-bearing glycans detected by AAL.

A model of glycosylated trimeric Env was generated to illustrate glycosite-specific alterations on CMU06-398F1 and CMU06-271.1 vs CMU06-WT (Fig 1E). Prominent changes were observed in glycan contents of N156 and N160 at the trimer apex (Fig 1E and F). N156 and N160 glycans constitute the TAMP and serve as key contacts for bnAbs such as PG9, PG16, PGT145 and PGDM1400 (19, 59, 60). On CMU06-WT Env, N156 was occupied by oligomannose (70%) and complex (19%) glycans, while 11% was unoccupied. In contrast, N156 was largely unoccupied on CMU06-398F1 (52%) and

CMU06-271.1 (83%). When N156 of CMU06-398F1 was occupied (48%), oligomannose glycans predominated at 45% and complex glycans constituted only 3%. The N173 glycan, which is recognized in place of N156 by PG9 on some HIV-1 isolates (61), is absent on CMU06 (Fig S2). N160 was decorated mostly by oligomannose glycans in CMU06-WT and CMU06-271.1 (81-82%) but had reduced abundance of oligomannose in CMU06-386F1 (71%). Complex-type glycans increased proportionally to 29% at N160 of CMU06-386F1 vs 19% in CMU06-WT and 18% in CMU06-271.1. At the nearby N188, also emanating from the apical V1V2 region, 398F1 and 271.1 SP swapping increased oligomannose glycans to 13% and 20%, respectively, from 0% in CMU06-WT.

Additional changes were also noted in glycans projecting laterally from the Env core at positions N295, N392, N407, N448, N462, and N465. N295 and N392, which together with N332/N334 comprise the IMP, had lower or higher proportions of complex glycans in SP-swapped viruses vs WT, whereas N332/N334 was detected in only CMU06-398F1 to contain oligomannose glycans. However, not all glycosites were affected by SP swapping; minimal to no changes were observed at N197, 94-100% of which was comprised of complex glycans, and at N398, which contained complex and oligomannose glycans at a ratio of ~1:2 in three tested Envs.

At the trimer base, N88 was largely unoccupied in CMU06-WT (82%) and CMU06-271.1 (82%) but had 50% occupancy in CMU06-398F1 with mainly oligomannose glycans. N611 and N616 at the trimer base in gp41 were 100% occupied by complex glycans in CMU06-WT and CMU06-398F1, but in CMU-271.1 oligomannose glycans were found at N611 (16%) and N616 (55%). The oligomannose content of N637 in gp41

increased from 69% in CMU06-WT to 89% in CMU06-271.1 but was reduced to 25% in CMU06-398F1. Glycosites at N135, N234, N241, N262, N276, N289, N356, N386 and N625 were undetectable in all three Envs.

Altered mAb recognition of CMU06 as a result of SP swapping.

Next, we examined the effect of SP swap on virus neutralization. Changes in sensitivity to neutralization were observed with each SP-swapped virus vs WT especially by V1V2 mAbs (Fig 2A-B). CMU06-CH119 and CMU06-271.1 were more resistant to neutralization by most V2i mAbs tested. Increased sensitivity to V2q mAbs PG9 and PG16 was observed for CMU06 with SPs from MW, 398F1, and 271.1. Neutralization of CMU06-WT by V3 crown-specific mAbs 2219 and 2557 was weak (AUC 13-16, IC50 >100 ug/ml). Switching SPs further reduced neutralization by 2219 and increased neutralization by 2557, except for MW SP which increased neutralization by both 2219 and 2557. Neutralization by V2p mAb CH59, gp41-MPER mAb (2F5), CD4bs mAbs, and CD4-IgG was unaltered (Fig 2A-B).

To evaluate the impact of SP swapping on Env antigenicity, we tested mAb binding to virus-derived gp120 captured onto ELISA plates and native Env expressed on the surface of 293T cells. ELISA with equivalent Env amounts showed reduced binding of all V2i mAbs tested to gp120 from CMU06-MW, CMU06-398F1, and CMU06-271.1, whereas binding to CMU06-CH119 gp120 was unaffected (Fig 2C). Considering that the viruses had an identical V1V2 sequence, the data indicated that SP swapping induced alterations of the V2i structure and/or exposure to reduce mAb recognition. Sporadic changes were also seen with V3 mAb reactivity, while no changes were seen with CD4bs mAb NIH45-46.

Next, we tested if SP swapping triggered antigenic changes on Envs expressed on the 293T cell surface. While NIH45-46 had comparable binding, indicating equivalent expression of all five Envs, differences were observed with V2i, V2p, and V2q mAbs (Fig. 2D). V2i mAb 830 had reduced binding to CMU06-MW, CMU06-398F1, and CMU06-271.1 vs CMU06-WT. Binding of V2i mAb 697 for CMU06-CH119 and CMU06-271.1 was also reduced. V2p mAb CH59 had greater binding to CMU06 with SPs from 398F1, CH119, and 271.1 vs CMU06-WT. Reactivity of V3 crown mAbs 2219 and 2557 was also altered, and gp41-specific mAb (98-6) had reduced reactivity with all SP-swapped Envs vs WT. In contrast, binding of V2q mAb PGDM1400 and gp120-gp41 interface mAb PGT151 to SP-swapped and WT Envs was comparable. Collectively, these data demonstrated that SP swapping altered Env antigenicity with conspicuous impact on V1V2 epitopes.

Effect of SP swapping on REJO Env incorporation, glycosylation and antibody recognition

To evaluate the effect of SP swapping on a different Env backbone, we swapped SP of REJO (clade B, T/F, tier 2 IMC) with SPs of MW (clade C, chronic, tier 1A), AA05 (clade B, acute), AC02 (clade B, acute), and NL4.3 (clade B, chronic, tier 1) (Fig 3A). SP swapping resulted in viruses with comparable infectivity to REJO-WT, except for REJO-MW which had reduced infectivity (Fig 3B). SPs of AA05, AC02 and NL4.3 increased total Env incorporation, while MW SP lowered Env incorporation. The amount of gp120 (lower band) in REJO-MW was also reduced by 90% (Fig 3C). The poor incorporation of cleaved functional Env into REJO-MW correlated with low infectivity of this virus.

We subsequently assessed the impact of SP switch on REJO Env glycosylation by lectin-probed Western blotting (Fig 3D). Comparable WT and SP-swapped total Env bands were detected by anti-gp120 mAbs. However, differences were observed with lectins (GNA and AAL) (Fig 3D). Compared with WT, the lower band of REJO-NL4.3 reacted more strongly with GNA (2.5-fold) and AAL (1.7-fold). Both GNA and AAL showed reduced binding to the upper band of REJO-AA05 and increased binding to the lower band of REJO-MW.

Similar to CMU06, neutralization was altered for SP-swapped REJO vs WT; however, the effect was most pronounced for REJO-AC02 and REJO-AA05 which became more resistant to 4 of 5 V2i mAbs and 1 of 4 V3 mAbs (Fig. 3E, F). REJO-AA05 was also more resistant to CD4bs mAb VRC01. Increased resistance to 2 of 5 V2i mAbs was similarly observed for REJO-NL4.3. REJO with AA05, AC02, and NL4.3 SPs became more resistant to V2q mAb PG9 (Fig. 3F), while neutralization by V2q mAb PGT145 was unaltered. V2p mAbs were not tested. In contrast, REJO-MW was more sensitive to V3 mAb 2219 and CD4bs mAbs VRC01 and 3BNC117.

To investigate the effect of SP swaps on REJO Env antigenicity, we assessed mAb binding to virus-derived gp120 (Fig. 3G) and Env expressed on 293T cells (Fig. 3H). Reduced binding of all V2i mAbs was seen with REJO-AC02. In contrast, binding of V3 mAbs, CD4bs mAb NIH45-46, and CD4-IgG to REJO-AC02 was unaltered. REJO-MW was excluded because of low gp120 content. When we examined mAb binding to native Env on 293T cells, a different pattern was observed. Lower binding of V2i, V3 and CD4bs mAbs was observed for one or more SP-swapped Envs. Swapping MW SP onto REJO Env almost abrogated the binding of trimer specific V2q mAb PGDM1400 and reduced

the binding of V2i mAbs 697 and 2158, without affecting the binding of V2p mAb CH59. As compared with REJO-WT, REJO-MW also displayed reduced reactivity with CD4bs mAbs NIH45-46 and 3BNC117, and V3 glycan-specific PGT121. In contrast, REJO-AC02, REJO-AA05, and REJO-NL4.3 had lower reactivity mainly with V2i (697 and/or 2158) and V3 (2219) mAbs. PGT151 mAb, which binds specifically cleaved Env trimer, showed increased binding to REJO-AC02, REJO-AA05, and REJO-NL4.3, while binding to REJO-WT and REJO-MW was comparable. Hence, like CMU06 SP swapping, REJO SP exchanges also modified mAb-Env interactions, most commonly with mAbs targeting V1V2 and occasionally with mAbs against V3 crown and CD4bs.

Strain-specific impact of SP swapping on SF162

To assess the consequences of SP exchanges on other virus strains, we generated SF162 viruses with WT and SP-swapped Envs (Fig. 4A). SF162 is a tier-1A neutralization-sensitive chronic clade B isolate. All SP-swapped and WT SF162 viruses displayed comparable levels of infectivity and Env incorporation (Fig. 4B, C). GNA and AAL reactivity demonstrated moderate changes of oligomannose and complex glycans on SP-swapped Envs vs WT (Fig. 4D). Neutralization by V2i and V3 mAbs was not markedly changed, except that SF162-MW was more sensitive to V2i mAbs 1357 and 1361 (Fig. 4E). SP-swapped SF162 viruses were also sporadically more sensitive to the CD4bs mAbs, and two of the viruses became more resistant to MPER gp41 mAb 2F5.

Figure 5 summarizes the differential effects of SP exchanges on neutralization phenotypes that depend on the Env backbones. Most pronounced effects were evident on neutralization by V1V2 mAbs: the SP swaps reduced neutralization sensitivity of CMU06 and REJO but had opposing effects on SF162. MW SP inflicted neutralization

sensitivity to many V2i, V2q, V3, and CD4bs mAbs, which varied depending on the Env backbones.

Host-cell dependence of SP impact on glycosylation and neutralization

Because glycosylation is host cell-dependent (62, 63), we investigated the effect of SP exchanges on CMU06 produced in primary $CD4^+$ T cells. PBMC-derived SP-swapped CMU06 viruses displayed a radically distinct neutralization pattern from 293T-produced counterparts (Fig 5, Fig 6 A-B). While 293T-derived SP-swapped CMU06 acquired increased resistance to V2i mAbs, PBMC-derived CMU06 with SPs from MW and 398F1 (both tier 1 isolates) became more sensitive to neutralization by most or all V2i mAbs. PBMC-derived SP-swapped viruses were also more resistant to V2q mAbs PG9 and PG16 and more sensitive to V2p mAb CH59, although neutralization by CD4bs mAbs was comparable. Contrastingly, CMU06-271.1 was more resistant to many V2i mAbs and MPER gp41 mAb 2F5, while swapping with CH119 SP did not alter neutralization by V2i and V2p mAbs and increased resistance to VRC01 (CD4bs) and 2F5 (MPER). The 271.1 and CH119 SPs are from tier 2 isolates. V3 crown mAbs had neutralization <50% against CMU06-WT; however, the SP-swapped viruses were even more resistant than WT.

SP swapping also altered the antigenicity of Env expressed on primary $CD4^+$ T cells. The changes were more drastic on SP-swapped CMU06 Envs expressed on $CD4^+$ T cells (Fig. 6C) vs 293T cells (Fig. 2D); the most prominent changes were detected with mAbs to V1V2. V2i and V2p mAbs bound CMU06-398F1, CMU06-CH119, and CMU06-271.1 less than CMU06-WT, but binding to CMU06-MW was unaltered or even increased. These SP-swapped viruses also showed reduced binding with V3 mAbs (2219 and 2557),

and CD4bs mAbs (NIH45-46 and 3BNC117), although binding of PGT151 was comparable. Collectively, the data show that SP swapping altered the antigenicity of native Env present on virions and cells, albeit in an Env strain- and host cell-dependent manner. Notwithstanding these variabilities, SP swapping clearly affects the V1V2 epitopes.

We further determined glycosylation changes on SP-swapped Envs from PBMC-produced CMU06 using lectin-probed Western blot. Unlike 293T-derived viruses (Fig 1D), we detected predominantly the lower gp120 bands with anti-gp120 mAbs (Fig 7A), suggesting host cell-specific differences in gp120/gp41 processing. Therefore, we analyzed GNA and AAL binding to the lower bands only. Moderate differences were observed in GNA and AAL binding to SP-swapped vs WT CMU06 (Fig 7A). However, the binding patterns were distinct from those seen with 293T-derived CMU06 (Fig 1D).

We also conducted glycosite-specific analyses of Envs from PBMC-grown viruses by LC-MS/MS (Fig. 7B-E). Of 28 N-glycosites in CMU06 gp160, we detected 16, 18 and 19 in CMU06-WT, CMU06-398F1 and CMU06-271.1, respectively. When the 15 glycosites detected in all three Envs were compared, the percentages of unoccupied glycans was higher in CMU06-WT (25%) and CMU06-398F1 (21%) compared to CMU06-271.1 (7%) (Fig. 7A-D, Supplementary Fig. 3). The oligomannose glycans were higher in CMU06-271.1 (48%) compared to CMU06-WT (34%) and CMU06-398F1 (33%). Likewise, total abundance of complex glycans was also altered in CMU06-WT (40%), CMU06-398F1 (47%) and CMU06-271.1 (45%).

Interestingly, the prominent change at N160 on the V1V2 apex was consistently noted in SP-swapped CMU06 produced in PBMCs and 293T cells (Fig. 1, 7,

Supplementary Fig. 3). N160 had a decreased oligomannose content upon 398F1 SP swapping, confirming that glycan alterations were incurred by 398F1 SP swap regardless of the producer cells.

We also assessed for glycans that were affected by both host cells and SPs; these comprised most N-glycans detected: N88, N150, N156, N188, N197, N295, N392, N407, N448, N462, N465, N611 and N616. Glycan content at these glycosites differed for PBMC- vs 293T-produced viruses and among the three SP-swapped viruses (Supplementary Fig. 3). Notably, N156 on the V1V2 apex displayed only oligomannose glycans in PBMC-derived CMU06-WT, but had a mix of oligomannose and complex glycans in 293T-derived CMU06-WT. On PBMC-derived CMU06-271.1, N156 also was completely occupied with oligomannose, whereas on 293T-derived counterpart it was mostly unoccupied. N156 had reduced oligomannose contents on CMU06-398F1 vs CMU06-WT and CMU06-271.1, when produced in PBMC or 293T cells. Another example is illustrated by N88 on the gp120-gp41 interface, which was completely unoccupied in PBMC-derived CMU06-WT, but 82% unoccupied in 293T-derived WT. In contrast, N88 was populated exclusively by complex glycans in CMU06-398F1 and CMU06-271.1 from PBMC, although it was 50% and 80% unoccupied in 293T-derived counterparts.

The N398 glycan changes depended on host cells only and independent of SPs. N398 was 100% occupied by complex glycans on all three PBMC-derived viruses, these were reduced to 22-36% in 293T-derived viruses.

Few glycosites were not identified in all samples, allowing only partial comparison. For example, N334 had only oligomannose glycans on all PBMC-derived viruses and 293T-derived CMU06-398-F1. N611 on gp41 was detected in two PBMC-derived and

three 293T-derived viruses and displayed exclusively or mostly complex glycans. N616 had complex glycans on four of five PBMC- and 293T-derived viruses but a mix of complex and oligomannose glycans on CMU06-271.1 from 293T cells.

Collectively, these data revealed the impact of SP changes on glycan compositions at specific glycosites and demonstrated the distinctive glycan profiles of viruses from PBMCs vs 293T cells. Because we compared viruses with identical Env sequences, the observed differences reflect how glycosylation proceeds at each glycosite in the context of different SPs and host cells.

Discussion

HIV-1 Env glycosylation is influenced by viral and cellular factors. This study demonstrates the effect of Env SP, a highly variable albeit understudied viral element, on glycosylation and consequently on Env properties and virus phenotypes. Introducing SPs from different virus strains to the same Env backbone altered proportions of oligomannose, complex, and unoccupied glycans on multiple glycosites. Interestingly, exchanging CMU06 SP with 398F1 SP reduced the oligomannose content of N156 and N160 glycosites, essential for several bNAbs, located on the V1V2 at the apex of the trimeric Env spike. This effect was observed in both PBMC and 293T-produced CMU06-398F1 viruses. Consistent with glycan changes, SP exchange affected Env recognition and virus neutralization by mAbs targeting V1V2 epitopes. Thus, although SP is not a part of the mature Env, it is a determinant that affects Env glycosylation and antibody recognition.

SP swaps impacted virus neutralization by V1V2-specific mAbs. Among the three classes of V1V2 mAbs, V2i mAbs were most prominently affected, as evidenced by increased resistance of many SP-swapped tier-2 CMU06 and REJO vs their respective WT to neutralization by V2i mAbs and not by mAbs against other Env regions. The effect nonetheless varied depending on SP and host cells used to produce the virus. Reasons for altered sensitivity to V2i mAb-mediated neutralization are not fully understood. The V2i epitopes are often occluded on native pre-fusion trimers of tier-2 viruses (22) and become exposed to mAbs only after prolonged virus-antibody incubation (14). The structural dynamics influencing V2i epitope exposure is governed partly by Env glycan composition. Our previous studies showed that enrichment of high-mannose glycans

375 increased virus resistance to V2i mAbs, even when the mAb-virus incubation was
376 extended to >18 hours (34). Here, we observed that the total oligomannose content was
377 increased by 4.4% and 7.9% on 293T-derived CMU06-398F1 and CMU06-271.1,
378 respectively, over that of CMU06-WT. The oligomannose content also increased by
379 15.5% on PBMC-derived CMU06-271.1. Correspondingly, these SP-swapped viruses
380 showed a trend of or a significant increase in V2i mAb resistance vs WT: the cumulative
381 neutralization AUC values decreased by 81 and 184 for 293T-derived CMU06-398F1 and
382 CMU06-271.1, respectively, and by 127 for PBMC-derived CMU06-271.1. In contrast, the
383 oligomannose content of PBMC-derived CMU06-398F1 was reduced by 4.2%, and the
384 virus was more sensitive to V2i mAbs (cumulative AUC of 504 vs 253 for WT). These
385 data suggest that increasing oligomannose glycans is one potential strategy that HIV-1
386 can employ to resist neutralizing activities of V2i Abs, and such alteration can be triggered
387 by changes in Env SP. Consistent with this, a single substitution in the N-terminal SP
388 region was found sufficient to affect Env glycan composition and increase virus resistance
389 to neutralization by V2i mAbs (34).

390 Unlike V2i mAbs, V2q mAbs PG9 and PG16 directly target oligosaccharide
391 moieties as part of their epitopes (64). Hybrid glycans bearing high mannose and
392 biantennary motifs with two terminal sialic acids at N156 and N160 on the V1V2 apex are
393 important for PG9 binding, whereas PG16 recognizes α-2,6-sialylated hybrid and
394 complex glycans on these sites (20, 65). Sensitivity of 293T-derived CMU06 to PG9 and
395 PG16 was enhanced when CMU06-WT SP was exchanged to MW, 398F1, or 271.1 SP.
396 In contrast, SP-swapped viruses were more resistant to V2q mAbs when produced in
397 PBMCs. Our LC-MS/MS data offered evidence for the first time that the modulation of

virus sensitivity to these V2q mAbs correlated with changes in the complex glycan content on the viruses. A decrease of complex glycans overall and at N156 and N160 collectively was observed in 293T-derived CMU06-398F1 and CMU06-271.1, both of which were more sensitive to V2q mAbs as compared to CMU06-WT. Conversely, the total complex glycan content and the proportion of complex glycans at N160 and N156 in combination increased when these viruses were grown in PBMC and the viruses became more resistant to V2q mAbs. These data indicate that an increased amount of complex glycans is unfavorable for V2q mAbs. Alternatively, the shift may supplant the hybrid-type glycan structures with terminal moieties preferred by these V2q mAbs (20, 65), but cannot be resolved by LC-MS/MS. Glycans proximal to N156 and N160, such as N136 and N149 (undetected here) also have been shown to influence the binding and neutralization by V2q mAbs (20, 66). More detailed studies are therefore required to define Env glycomes compatible with V2q mAbs.

In contrast to V2i and V2q mAbs, mAbs against other Env regions were less affected by SP swapping. Env binding and virus neutralization by CD4-IgG were likewise unaffected, indicative of the proper folding of all tested SP-swapped Envs. The SP-swapped Envs also maintained the features characteristic of the native trimeric Env, such as the presence of TAMP, which is absent on uncleaved or incorrectly assembled trimers (67-69), and the exclusive oligomannose content at N276 when this glycosite was detected (PBMC-produced CMU06-WT and CU06-271.1). This contrasted to the N276 occupation by complex glycans on BG505 pseudotrimers and gp120 monomers (67). Further, we observed no drastic reduction of PGT151 mAb binding to SP-swapped vs WT Envs, and three SP swaps even increased PGT151 binding to REJO Env. PGT151, which

targets glycan-bearing epitopes in the gp120-gp41 interface like mAb 35O22, binds only to properly folded, cleaved trimers (70, 71). Similarly, Env binding and virus neutralization by trimer-dependent V2q mAbs PGT145 and PGDM1400 were largely undisturbed by SP exchanges, except for REJO-MW. We also observed only minimal sporadic effects on neutralization by V3 crown mAbs, demonstrating that SP swapping did not shift Env trimers toward more open conformations (72-74). Altogether, these data indicate that SP swapping subtly modifies the proportion of Env oligosaccharide content and the antigenicity of V1V2 without triggering global structural transformations on Env.

As indicated by comparable Env incorporation and virus infectivity, SP exchanges had no deleterious effects on Env functions. One exception was REJO-MW, which diminished expression of functional cleaved Env gp120, reduced Env incorporation into virions, and decreased virus infectivity. However, this effect was not seen when MW SP was introduced to CMU06 and SF162. The reasons for REJO-MW incompatibility remains unclear. A reduction of cleaved gp120 was previously noted when a mutation was introduced to position 12 of REJO SP (H12Q), but not to that of JRFL SP (Y12Q) (34). Glutamine occupies position 12 of MW SP and not the other SPs tested with REJO, but MW SP also differs from REJO SP at 9 other positions, requiring systematic evaluations for the contribution of glutamine at position 12 vs other MW SP residues.

Glycosylation begins in the ER with the addition of Glc3Man9GlcNAc2 onto asparagine in the NX(T/S) (X≠Proline) sequon on a nascent protein. As the protein crosses the ER and the Golgi apparatus, the high-mannose structure is trimmed and subsequently elaborated with hybrid- and complex-type glycans. In view of the observed effect of SP swapping, we suggest that the extent to which the glycan on a particular

glycosite is processed is decided while Env is an ER resident with its SP still tethered. SP may subtly affect the compactness of Env folding, which consequently imposes or releases structural constrains to enzymes that generate hybrid or complex glycans in the Golgi. Nonetheless, the steps at which the SP sequence dictates the glycan content of Env are unknown. The Env SP is cleaved post-translationally and this delayed SP cleavage is seen across HIV-1 subtypes ensuring low Env expression on virions (5, 6, 75). In addition to the positively charged n-region, residues in the hydrophobic SP region (h-region) and downstream of the SP cleavage site are important for this property (5, 6). The h-region forms an alpha-helix across the ER membrane and covers the cleavage site to delay SP cleavage (3, 5). Since the cleavage sites in SP-swapped Envs and WT counterparts are identical, perhaps the h-region variations affect the cleavage site accessibility for signal peptidase, altering the efficiency of SP cleavage of Env with heterologous SPs, similar to that seen with the h-region-mediated regulation of SP cleavage for preprolactin (76, 77).

Prediction based on Model SignalP 3.0 (78) indicates that the cleavage probabilities increased for CMU06 with 398F1, CH119, and 271.1 SPs vs WT (Fig S4 A-B), with 271.1 SP having the highest probability. Topology and structure predictions using PSIRED (79, 80) further show differences in the cytoplasmic and ER regions and in the alpha-helical structure around the cleavage site (Fig S4 C-D). The transmembrane-spanning residues encompass positions 16-31 for CMU06 WT and CMU06-CH119 but differ for the other three swaps. The 271.1 SP cleavage site is also shown to be most exposed (Fig S4 D), but experimental data are needed to verify if cleavage efficiency is indeed changed to affect the rate of Env synthesis. Past studies demonstrated, however,

that replacing SPs of influenza hemagglutinin and HIV-1 Env by tPA/22P SP, which increased SP cleavage probability to 0.925, caused higher secretion of these proteins (81). Similarly, M26P mutation in HIV-1 HXB2 SP was found to increase the SP cleavage probability from 0.628 to 0.928 and change the SP cleavage from post-translational to co-translational (6). Prolines are notably absent near SP cleavage sites in 99.9% of HIV-1 gp160 (6).

In additional to SP cleavage, SP interaction with the signal-recognition particle (SRP) may also play a role in determining Env phenotypes. The h- and n-regions, which vary greatly among SPs in length and sequence, are deemed important for SRP interaction (82-84). Thus, it is possible that different SPs may bind SRP with different affinities impacting the chaperone-mediated Sec61 channel gating and the interaction with chaperones involved in protein folding and assembly (76, 85, 86). A single substitution of a helix-breaking glycine residue by a helix-promoting leucine residue in the hydrophobic core of prokaryotic SPs can promote SRP binding (87, 88) and regulate the pathway of protein translocation (89). The SPs studied here differ in the number of basic, hydrophobic, and leucine residues (Fig S1); the significance of each element needs to be better understood, considering that SP exchange is a common strategy to promote secretion of recombinant Env vaccines and SP selection is critical to generate glycomes faithfully representing those of native Envs.

In summary, this study demonstrates an important role of HIV-1 Env SP in influencing Env glycan content. By introducing SP from a particular HIV-1 strain, we can modulate the relative proportion of unoccupied, high-mannose, and complex glycans on specific glycosites, including those on V1V2 at the apex of Env spike. SP swap also can

alter Env recognition and virus neutralization by mAbs, especially mAbs against V1V2. Data from this study have significant implications for vaccine development: SP is a critical component that must be rationally selected and incorporated into the design of Env-based HIV-1 vaccine.

Acknowledgements

The authors thank Ms. Vincenza Itri and Ms. Xiaomei Liu for providing HIV-1-specific mAbs and Ms. Alisa Fox for assistance with flow cytometry. This study was supported in part by NIH R01 grant (AI140909 to C.U.), NIH R21 grant (AI124863 to C.U. and C.E.H.), NIH R01 (AI145655) to X-P.K, VA Merit Review Award (I01BX003860 to C.E.H.) and VA Research Career Scientist Award (1IK6BX004607 to C.E.H). The funders had no role in study design, data collection and analysis, decision to publish, or preparation of the manuscript.

Author Contributions

Conceptualization, C.U.; Supervision: C.U.; Investigation, C.U., R.F, L.C, K-W. C, K.L., W.Y., and J.Y.; Formal Analysis: C.U., A.N.; Resources: J.A, S.Z-P., H.Z., and X-P. K.; Writing – Original Draft, C.U.; Writing – Review & Editing, C.U., and C.E.H; Funding Acquisition, C.U and CEH.

Declaration of Interests

The authors declare no competing interests.

Figure legends

Figure 1. Effect of SP swap on CMU06 Env glycosylation

(A) CMU06 WT and swapped SPs. SP cleavage site is denoted by red triangle.

(B) Infectivity of WT vs SP-swapped CMU06 in CD4+ TZM.bl cells. Viruses were produced in 293T cells.

(C) Measurement of WT vs SP-swapped Env incorporation into CMU06 virions produced in 293T cells by Western blot. A gp120 mAb cocktail and a p24 Gag mAb were used. Levels of Env incorporation were based on Env/p24 ratios (WT=100%).

(D) Assessment of Env glycan content by lectin-probed Western blotting. Comparable amounts of Envs from 293T-produced sucrose-pelleted virions were separated by SDS-PAGE, blotted, and probed with a gp120 mAb cocktail or lectins (GNA and AAL). Density of upper and lower Env bands (grey and black arrows) were measured.

(E) Top panel: Env trimer models (generated using a SOSIP.664 trimer PDB 5FYJ) showing the predominating glycoforms at each of the CMU06 glycosites for CMU06-WT, CMU06-398F1, and CMU06-271.1. Type of glycans added was based on LC-MS/MS data of virion-associated Envs from 293T cells (bar graphs, bottom panel).

Bottom panel: Relative amounts of unoccupied, oligomannose, and complex glycans at glycosites on SP-swapped vs WT CMU06 as determined by LC-MS/MS. nd: glycosites not detected in 1 or 2 Envs.

(F) Changes in glycan content at each glycosite for CMU06-398F1 and CMU06-271.1 vs CMU06-WT calculated from Figure 1E data.

Figure 2. Effect of SP swap on CMU06 Env-antibody interaction

(A) Neutralization of 293T-derived CMU06. Viruses were incubated with titrated mAbs at 37°C for 24 hours before addition of TZM.bl cells, except for PG9, NIH45-46, VRC01, 3BNC117, 2F5 and CD4-IgG which were pre-incubated with viruses for 1 hour. MAb 1418 served as negative control. Representative neutralization curves are shown. Mean and SEM from 2-3 experiments are shown.

(B) Neutralization AUCs (areas under the curves) of WT vs SP-swapped CMU06 with different mAbs.

(C) ELISA binding of mAbs to gp120 derived from CMU06-WT vs SP-swapped viruses. MAbs were titrated ten-fold from 10 µg/ml, while CD4-IgG was titrated five-fold from 10 µg/ml. AUC values are shown.

(D) Binding of mAbs to WT vs SP-swapped Envs expressed on the surface of 293T cells. MAbs were tested at following concentrations: 697, 830 and 3685 at 100µg/ml; 2G12 at 50µg/ml; PGDM1400, 2219, 2557, 240D, 98-6 and PGT121 at 25µg/ml; b12 at 20µg/ml; 4E10, 17b at 10µg/ml; PGT128, PGT151, 3BNC117 and CD4-IgG at 5µg/ml; CH59 and NIH45-46 at 2.5µg/ml. Geometric mean fluorescence intensity (MFI) and SD from duplicates in one experiment are shown.

Data were analyzed by 2-way ANOVA (* $p < 0.05$, ** $p < 0.01$, vs WT).

Figure 3. Effects of SP swap on REJO

(A) REJO WT and swapped SPs. Red triangle: SP cleavage site. -, undetermined.

(B) Infectivity of WT vs SP-swapped REJO from 293T cells in TZM.bl cells. *, $p = 0.01$ vs WT by Mann-Whitney test.

(C) Measurement of Env incorporation into virions by Western blot as in Fig 1C. *, $p \leq 0.005$ vs WT by unpaired t-test.

(D) Analysis of REJO Env glycosylation by lectin-probed Western blotting as in Fig 1D.

(E) Neutralization of WT and SP-swapped REJO treated with titrated amounts of anti-Env mAbs. Neutralization was performed as in Fig 2A-B. Data for V2i mAb 1361 and V2q mAb PG9 are shown. **, $p < 0.001$ vs WT by 2-way ANOVA.

(F) Neutralization AUCs of WT vs SP-swapped viruses with different mAbs. NT, not tested.

(G) ELISA binding of mAbs and CD4-IgG to gp120 from WT and SP-swapped viruses. Titration was done as in Fig 2D and AUCs are shown. *, $p < 0.05$ vs WT by ANOVA of the titration curves.

(H) Binding of mAbs to REJO WT vs SP-swapped Envs expressed on the surface of 293T cells. MAbs were tested at concentration: 697, 2158 and 3685 at 100µg/ml; 2219 and 2557 at 50µg/ml; PGT128, PGT121 and 35O22 at 25 µg/ml; CH59, 3BNC117 at 20µg/ml; PGDM1400 and PGT151 at 10µg/ml; NIH45-46 at 2.5µg/ml. Averages and SEM of MFI from duplicates of two experiments are shown. *, $p < 0.05$; ** $p < 0.01$ vs WT by 2-way ANOVA.

Figure 4. Effects of SP swap on SF162

(A) SF162-WT and swapped SPs. Red triangle: SP cleavage site.

(B) Infectivity of 293T-derived SF162 WT vs SP-swapped viruses in TZM.bl cells.

(C) Measurement of Env incorporation by Western blot as in Fig 1C. *, $p = 0.017$ vs WT by unpaired t-test.

(D) Binding of Env from SF162 WT and SP-swapped viruses by gp120 mAbs and lectins (GNA and AAL) in Western blots. Densities of upper and lower Env bands (gray and black arrows) are shown.

(E) Neutralization AUCs of WT vs SP-swapped viruses with different mAbs. NT, not tested.

Figure 5. Changes of neutralization sensitivity in the context of different Envs and SPs. AUC changes relative to the respective WT were calculated: (SP-swapped AUC – WT AUC). NT, not tested.

Figure 6. Effect of SP swap on neutralization of CMU06 produced in PBMCs and antigenicity of CMU06 Env expressed on human CD4$^+$ T cells

(A) Virus neutralization was measured using TZM.bl cells. MAb 1418 served as a negative control. Neutralization curves of selected virus-mAb pairs are shown. *, $p < 0.05$, **, $p < 0.01$, ***, $p < 0.001$, vs WT by 2-way ANOVA

(B) Neutralization AUCs of WT vs SP-swapped viruses by different mAbs.

(C) Binding of mAbs to Env expressed on CD4$^+$ T cell surface. MAbs were tested at the concentrations: 697, 830, 2219 and 2557 and 3685 at 100µg/ml; PGT121 25µg/ml; CH59 and PGT151 at 10µg/ml; NIH45-46 at 2.5µg/ml; 3BNC117 at 20µg/ml. MFI and SD from duplicates of one experiment are shown. *, $p< 0.05$ vs WT by ANOVA.

Figure 7. Changes in glycosylation on Env of CMU06 WT and SP-swapped viruses produced in PBMC

(A) Binding of Env by mAbs and lectins (GNA and AAL) measured in Western blots.

(B–D) Top panel: Models of glycosylated Env trimers from PBMC-derived CMU06 WT and SP-swapped viruses. Models and glycans were generated as in Fig 1E. Bottom panel: Proportions of unoccupied, oligomannose, and complex glycans at each glycosite. Glycosites undetected in all 3 Envs are not shown. nd: not detected in 1 or 2 Envs.

Supplementary Figure Legends

Figure S1. Sequence alignment of all Env SPs tested in this study. -, undetermined. Amino acid sequence alignment made using the Lasergene DNASTAR Megalign software.

Figure S2. CMU06 gp160 sequence. N-glycosylation sites (red) are marked throughout the entire gp160 sequence that encompasses SP, constant regions (C1-C5), variable regions (V1-V5), and gp41.

Figure S3. Glycan contents at glycosites on CMU06-WT (A), CMU06-398F1 (B), and CMU06-271.1 (C) produced in PBMCs vs 293T cells. Glycosites detected on at least one of the Envs from PBMCs- and 293T-derived viruses are shown. (D) Percentages of unoccupied, complex, and oligomannose glycans on gp120 and gp41 from viruses grown in 293T cells vs PBMCs. ND: not detected.

Figure S4. SP prediction. (A) SP prediction tool SignalP 3.0 applied to SPs of CMU06 WT and swap variants. Vertical red bars show the first amino acid after the cleavage site. (B) Probability of SP cleavage predicted by SignalP3.0. (C-D) PSIPRED-predicted MEMSAT-SVM helix orientation models (C) and DMPFold structures (D) of CMU06 WT and swapped SPs. One of the 5 structures predicted by PSIPRED is shown for each SP (D). α-helices: cyan, loops: magenta, residues C27, A29 and D31 around the cleavage site: magenta sticks.

Materials and methods

Plasmids

The infectious molecular clones (IMC) were generated by cloning the CMU06 and SF162 Envs into pNL4.3 backbone to construct pNL-CMU06 and pNL-SF162, respectively. To generate SP-swapped CMU06 IMCs, restriction site NheI was introduced at positions 89-90 (CGGAGT to GCTAGC) without amino acid alterations (A29, S30). DNA fragments with swapped SPs were synthesized (Genscript) and digested using EcoRI (in pNL4.3 backbone) and NheI and ligated to pNL-SF162 and pNL-CMU06 digested with the same enzymes. The pREJO.c/2864 IMC (REJO) was used to make REJO SP-swapped plasmids by a multi-step overlapping PCR mutagenesis strategy using Pfx50™ DNA Polymerase PCR System (34). Briefly, in the first PCR step, mutated fragments were individually generated in two separate reactions. The primer pairs AvrIIF/MWR and MWF/BstEIIR were used to generate pREJO-MW (STAR Methods). The PCR fragments were agarose gel-purified, combined, and added to a second-stage PCR with the flanking primers AvrIIF and BstEIIR. Products of the second-stage PCR were digested by AvrII and BstEII restriction enzymes and inserted into the AvrII- and BstEII-digested fragment of pREJO.c/2864 to yield REJO-MW. The other REJO plasmids were constructed similarly using the primers listed in STAR Methods. All the plasmids were sequenced to confirm the presence of the desired sequence changes without any other mutations.

Cell lines

HEK293T/17 cells (293T) were used to produce infectious HIV-1 viruses. TZM.bl cell line was used to assay virus infectivity and virus neutralization. TZM.bl cell line is derived from HeLa cells and genetically modified to express high levels of CD4, CCR5 and CXCR4

and contain reporter cassettes of luciferase and β-galactosidase that are each expressed from an HIV-1 LTR. The 293T and TZM.bl cell lines were routinely subcultured every 3 to 4 days by trypsinization and were maintained in Dulbecco's modified Eagle's medium (DMEM) supplemented with 10% heat-inactivated fetal bovine serum (FBS), HEPES pH 7.4 (10 mM), L-glutamine (2 mM), penicillin (100 U/ml), and streptomycin (100 µg/ml) at 37ºC in a humidified atmosphere with 5% CO2.

Viruses

Infectious viruses were generated by transfecting 293T cells with wild type (WT) or SP-swapped pNL-CMU06, pREJO and pNL-SF162 plasmids using jetPEI transfection reagent (34). Supernatants were harvested after 48 hours and clarified by centrifugation and 0.45µm filtration. Single-use aliquots were stored at −80°C until use. Virus infectivity was assessed on TZM.bl cells as described (34, 90). Briefly, serial two-fold dilutions of virus stock in 10% DMEM were incubated with TZM.bl cells (in duplicates for each dilution) in half-area 96-well plate in presence of DEAE-Dextran (12.5 µg/ml) for 48 hours at 37ºC. Virus infectivity was measured by β-galactosidase activity. The dilution of a virus stock that yielded RLUs between 150,000 and 200,000 was used in neutralization assays, as detailed below. HIV-1 p24 ELISA assay was used to quantify the p24 content in each virus stock using the manufacturer's protocols.

To generate PBMC-derived viral stocks, PBMC were isolated by lymphoprep gradient centrifugation from leukopaks of HIV-1 seronegative donors. Prior to HIV-1 infection, PBMC were activated by incubation in RPMI-intereukin-2 (IL-2) growth medium containing 10 µg of phytohemagglutinin (PHA) (PHA-P) per ml. The RPMI-IL-2 growth medium was RPMI 1640 medium supplemented with 10% heat-inactivated fetal calf

serum, L-glutamine (2 mM), penicillin (100 U/ml) and streptomycin (100 µg/ml) and 20 U of recombinant IL-2 per ml. After overnight incubation with PHA, cells were washed and cultured with IL-2 for additional 2 to 3 days. All cultures were maintained in 5% CO2 incubators at 37°C. PBMCs were exposed to virus (50ng p24 of 293T-derived stock) overnight and then washed to remove the viral inoculum. Virus-containing supernatant was harvested on day 7 and day 10. Virus infectivity and p24 contents were measured as above.

Human monoclonal antibodies. V2i, V3, and control mAbs were produced in our laboratory as described (26, 91-97). Other mAbs used in this study were obtained through the NIH AIDS Reagent Program, Division of AIDS, NIAID, NIH. MAbs specific to different Env epitopes were tested, including: V2i (697, 1357, 1361, 1393 and 2158), V2p (CH59), V2q (PG9, PG16, PGT145 and PGDM1400), V3 (2219, 2557, 3074 and 3869), CD4bs (NIH45-46, VRC01, b12, 3BNC117), CD4i (17b), glycan dependent (PGT121, PGT128 and 2G12), gp41 (240-D, 98-8, 2F5 and 4E10), and gp120-gp41 interface (PGT151 and 35O22). An CD4-IgG fusion protein was also included, along with an irrelevant anti-parvovirus mAb 1418 and anti-anthrax mAbs 3685 used as negative controls.

A cocktail of anti-human anti-gp120 mAbs (anti-V3: 391, 694, 2219, 2558; anti-C2: 846, 1006; anti-C5: 450, 670, 722, 1µg/ml each) were used to detect Env. The mAb 91-5D (1µg/ml) was used to detect Gag p24.

Virus neutralization assay. Neutralization activity of HIV-1-specific antibodies was measured as a reduction in β-galactosidase reporter gene expression of TZM-bl cells after infection of TZM-bl cells with WT and SP-swapped viruses. Neutralization was performed using either the standard 1 hour assay (14, 34, 98) or the prolonged 24 hour

assay (14, 98). Serially diluted antibodies and viruses (150,000-200,000 RLUs) were pre-incubated for 1 hour or 24 hours prior to adding the target TZM.bl cells. After a 48-hour incubation at 37ºC and 5% CO2 incubator, the β-galactosidase activity was measured. Each condition was tested in duplicate or triplicate, and experiments were repeated 2-4 times. Percent neutralization was determined based on virus control (TZM.bl cells with virus alone) and cell control (TZM.bl cells only) under the specific assay condition. Neutralization assays were performed after a 24-hour mAbs-virus incubation for all mAbs except PG9, PGT145, NIH45-46, VRC01, 3BNC117, and CD4-IgG which were pre-incubated with viruses for 1 hour.

Western blot analyses with antibodies and lectin probes. Western blot analyses were performed to quantify the ratios of Env to p24 proteins incorporated into the WT and SP-swapped viruses and to evaluate Env reactivity with different lectins as in (34). The virus particles sucrose-pelleted from supernatants were lysed in SDS-PAGE loading buffer, resolved on 4–20% tris-glycine gels, and blotted onto nitrocellulose membranes, blocked overnight with 5% skim milk powder in phosphate buffered saline (PBS) followed by probing with antibodies or lectins. A cocktail of anti-human anti-gp120 mAbs (anti-V3: 391, 694, 2219, 2558; anti-C2: 846, 1006; anti-C5: 450, 670, 722, 1µg/ml each) were used to detect Env. The mAb 91-5D (1µg/ml) was used to detect Gag p24. Biotinylated GNA, and biotinylated AAL were each used at 2µg/ml. Lectin binding was detected with HRP-neutravidin (1:1500 for 1 hr RT). All dilutions were made in Superblock T20 Buffer. Membranes were developed with Clarity Western ECL substrate and scanned by ChemiDoc Imaging Systems (Bio-Rad Laboratories). Purified recombinant gp120 and

p24 proteins were also loaded at a known concentration as controls (data not shown). Band intensities were quantified using the Image Lab Software Version 5.0.

gp120 – mAb binding assay. The relative binding of mAbs to gp120 from WT and SP-swapped viruses was measured by a sandwich ELISA. Half-area high-binding ELISA plates were coated with sheep anti-C terminal gp120 Abs (1µg/ml in PBS), blocked with 2% bovine serum albumin (BSA) in PBS, and incubated with 1% Triton X100-virus lysates containing 20 ng/ml Env (quantitated by Western blots). Serially diluted mAbs (0.01-10µg/ml) were then added for 2 hours, and the bound mAbs were detected with alkaline phosphatase-conjugated goat anti-human IgG and p-nitrophenyl phosphate substrate. The optical density (OD) was read at 405nm using BioTek PowerWave HT Microplate Spectrophotometer.

Cell-associated Env binding assay. Assay to detect antibody binding to cell surface-expressed Env was performed as described (99) with minor modifications. A total of 4×10^6 293T cells were seeded in 15 ml of culture medium in a 100-mm tissue culture dish and incubated at 37 °C. Twenty four hours later, cells in each dish were transfected with 20 µg gp160 expression plasmid (WT or SP swaps) using JetPEI (DNA:JetPEI ratio of 1:3) following manufacturer's instructions. The transfected cells were incubated for 24 hours at 37 °C, washed with PBS, detached with trypsin-free cell-dissociation buffer, and resuspended in PBS containing 2% BSA. Cells were stained with Live/dead Aqua stain and distributed into 96-well round-bottom tissue culture plates ($5x10^4$/well) for individual staining reactions. Cells were incubated with mAbs at concentrations detailed in figure legends. For detection of mAb binding, biotinylated goat anti-Human IgG Fc (1:1000) followed by streptavidin phycoerythrin (PE) (1:500) was used. The cells were washed 3X

with PBS-B (PBS plus 1%BSA) after each step and all incubation steps were performed on ice for 30 min. Cells were analyzed with a BD Fortessa flow cytometer, and 30,000 events were collected in the PE+ gate. Analysis was carried out using FCS-Express software as follows: 293T cells were selected from a plot of forward-area vs. side scatter-area (FSC-A/SSC-A) from which doublets were excluded in a forward scatter height vs forward scatter area plot (FSC-H/FSC-A). Live cells were selected by Aqua-negative gating, and geometric mean fluorescent intensity (MFI) of PE+ cells, representing anti-Env-stained cells, were quantified. Background MFI, as determined from cells stained without primary antibodies was subtracted from all Env-mAb pairs.

For testing mAb binding to Env expressed on primary CD4+ T cells, the experiments were conducted as above with the following modifications: CD4+ T cells were isolated from PBMCs (isolated from Leukopaks) using an EasySep Human CD4+ T cell Enrichment Kit. PHA-activated CD4+ T cells were infected with WT or SP-swapped viruses (500 ng p24/million cells) by spinoculation at 1200×g for 2 hours. The virus inoculum was replaced with fresh medium (RPMI 1640 media supplemented with 10% FBS with 20 U/mL IL-2) and the cells were further incubated for 7 days at 37°C. Cells were harvested for mAb staining as above.

Mass Spectrometry: Analysis for site-specific glycosylation was performed as in (100). Briefly, 293T- and PBMC-derived infectious virus stocks were concentrated by sucrose cushion centrifugation. Concentrated (250X) virus preparations were loaded on SDS-PAGE gel (7.5%) and the separated Env bands were excised to use directly for mass spectrometry (MS).

The SDS-PAGE gel bands were washed with 100% acetonitrile and water three times. A proteomics-based strategy was used to assess the degree of glycan processing and the degree of site-occupancy of each glycosite (100). The proteins in the gel bands were denatured and alkylated by 10 mM dithiothreitol (DTT) and 55 mM iodoacetamide in 25 mM ammonium bicarbonate, respectively. The resulting proteins were digested with the combination of trypsin and chymotrypsin at an enzyme/substrate ratios of 1:15 (w/w) and 1:10 (w/w) respectively in 25 mM ammonium bicarbonate. Sequential treatment with two endoglycosidases was then performed to introduce novel mass signatures for peptides that contain glycans of high-mannose types and complex-type glycans (100). First, the Env peptides were digested with Endo H to cleave high-mannose (and hybrid) glycans between the innermost GlcNAc residues, leaving a GlcNAc attached to the Asn (N+203). The subsequent PNGase F treatment removed the remaining complex-type glycans, and in the process converted Asn to Asp, resulting in a +0.984 Da mass shift (N+1) (101, 102). For peptides with unoccupied glycosites, these treatments produce no mass shift (N+0). Using this strategy, liquid chromatography–mass spectrometry (LC-MS/MS) data were acquired for each sample. Peptides were identified using SEQUEST. The abundance of each peptide was determined by the sum of the peak areas from all identified charge states (64).

The 293T-derived Env samples were analyzed on a Q-Exactive mass spectrometer. De-glycosylated peptides were separated on a Dionex Ultimate 3000 RSLC nano system with a 75 µm × 15 cm Acclaim PepMap100 separating column protected by a 2-cm guard column. The flow rate was set at 300 nl/min. Buffer A and B were 3% ACN (0.1% FA) and 90% ACN (0.1% FA), respectively. A 130-minute gradient

was run, consisting of the following steps: 0-10 min, 2-5% B; 10-90 min, 5-25% B; 90-112 min, 25-35% B; 112-115 min, 35-95%; 115-125 min, hold at 95% B; 125-129 min, 95-2% B; 129-130 min, hold at 2% B. Orbitrap MS1 spectra (AGC 3e6) were collected from 400–1,800 m/z at a resolution of 70 K followed by data dependent higher-energy collisional dissociation tandem mass spectrometry (HCD MS/MS) (resolution 35,000 and collision energy 31%) of the 12 most abundant ions using an isolation width of 1.4 Da. Dynamic exclusion time was set at 30s.

The PBMC-derived Env samples were analyzed on an Orbitrap Fusion Lumos tribrid mass spectrometer. Approximately 1 µg of de-glycosylated peptides were injected directly onto a 28 cm, 75 um ID column packed with 1.9 um Reprosil-Pur C18-AQ beads (Dr. Maisch GmbH). The flow rate was separated at 300 nl/min on an EASY-nLC 1200. Buffer A and B were 3% ACN (0.1% FA) and 90% ACN (0.1% FA), respectively. A 110-minute gradient was run, consisting of the following steps: 0-1 min, 2-6% B; 1-85 min, 6-30% B; 85-94 min, 30-60% B; 94-95 min, 60-90% B; 95-100 min, hold at 90% B; 100-101 min, 90-50% B; 101-110 min hold at 50% B. Peptides were eluted directly from the tip of the column and nanosprayed into the mass spectrometer. The Orbitrap Fusion Lumos was operated in a data-dependent mode. Full MS1 scans were collected in the Orbitrap at 60 K resolution with a mass range of 350–2,000 m/z and an AGC target of 4e5. The cycle time was set to 2 s, and within this 2 s the most abundant ions per scan were selected for CID MS/MS in the orbitrap with an AGC target of 5e4. Maximum injection times were set to 50 ms for both MS and MS/MS scans. Monoisotopic precursor selection was enabled, and dynamic exclusion was used with exclusion duration of 45 s.

CMU06 Env trimer model was generated using a SOSIP.664 trimer (PDB 5FYJ) at each glycosite, except N651 due to lack of template. Glycan was added onto models based on the LC-MS/MS data of virion-associated Envs from 293T cells and PBMC. For sites with high complex-type content, biantennary glycan with core fucose Gal2GlcNAc2Man3FucGlcNAc2 moieties were used. For those with high oligomannose content, Man5GlcNAc2 was added. Protein surface and glycans that were undetermined or absent on CMU06 were colored gray. Glycosites at N135, N234, N241, N262, N276, N289, N356, N386 and N625 were undetected in all Envs and are not shown.

CMU06 Env trimer protein model was generated using a SOSIP.664 trimer (PDB 5FYJ). Glycans were added onto the model based on the LC-MS/MS data of virion-associated Envs from 293T cells except glycan N674 due to the lack of a template. For glycosites with high complex-type content, biantennary glycans with core fucose Gal2GlcNAc2Man3FucGlcNAc2 moieties were used. For those with high oligomannose content or undetected, Man5GlcNAc2 were added. Glycans that were undetected (e.g., N135, N234, N241, N262, N276, N289, N356, N386 and N625) are colored gray, while those that were unoccupied on PBMC-derived CMU06 are displayed by semi-transparent yellow patches.

Statistical analysis. Comparison of SP swaps vs WT groups and controls was done using analysis of variance (ANOVA) or by Student’s t-test as mentioned in the figure legends. Statistical analyses were performed with GraphPad Prism 8.

References

1. Haeuptle MT, Flint N, Gough NM, Dobberstein B. A tripartite structure of the signals that determine protein insertion into the endoplasmic reticulum membrane. J Cell Biol. 1989;108(4):1227-36.
2. Land A, Braakman I. Folding of the human immunodeficiency virus type 1 envelope glycoprotein in the endoplasmic reticulum. Biochimie. 2001;83(8):783-90.
3. Li Y, Bergeron JJ, Luo L, Ou WJ, Thomas DY, Kang CY. Effects of inefficient cleavage of the signal sequence of HIV-1 gp 120 on its association with calnexin, folding, and intracellular transport. Proceedings of the National Academy of Sciences of the United States of America. 1996;93(18):9606-11.
4. Li Y, Luo L, Rasool N, Kang CY. Glycosylation is necessary for the correct folding of human immunodeficiency virus gp120 in CD4 binding. Journal of virology. 1993;67(1):584-8.
5. Li Y, Luo L, Thomas DY, Kang CY. Control of expression, glycosylation, and secretion of HIV-1 gp120 by homologous and heterologous signal sequences. Virology. 1994;204(1):266-78.
6. Snapp EL, McCaul N, Quandte M, Cabartova Z, Bontjer I, Kallgren C, et al. Structure and topology around the cleavage site regulate post-translational cleavage of the HIV-1 gp160 signal peptide. eLife. 2017;6.
7. Checkley MA, Luttge BG, Freed EO. HIV-1 envelope glycoprotein biosynthesis, trafficking, and incorporation. Journal of molecular biology. 2011;410(4):582-608.
8. Julien JP, Cupo A, Sok D, Stanfield RL, Lyumkis D, Deller MC, et al. Crystal structure of a soluble cleaved HIV-1 envelope trimer. Science. 2013;342(6165):1477-83.
9. Lyumkis D, Julien JP, de Val N, Cupo A, Potter CS, Klasse PJ, et al. Cryo-EM structure of a fully glycosylated soluble cleaved HIV-1 envelope trimer. Science. 2013;342(6165):1484-90.
10. Pancera M, Zhou T, Druz A, Georgiev IS, Soto C, Gorman J, et al. Structure and immune recognition of trimeric pre-fusion HIV-1 Env. Nature. 2014;514(7523):455-61.
11. Gottardo R, Bailer RT, Korber BT, Gnanakaran S, Phillips J, Shen X, et al. Plasma IgG to linear epitopes in the V2 and V3 regions of HIV-1 gp120 correlate with a reduced risk of infection in the RV144 vaccine efficacy trial. PloS one. 2013;8(9):e75665.
12. Karasavvas N, Billings E, Rao M, Williams C, Zolla-Pazner S, Bailer RT, et al. The Thai Phase III HIV Type 1 Vaccine trial (RV144) regimen induces antibodies that target conserved regions within the V2 loop of gp120. AIDS Res Hum Retroviruses. 2012;28(11):1444-57.
13. Zolla-Pazner S, Edlefsen PT, Rolland M, Kong XP, deCamp A, Gottardo R, et al. Vaccine-induced Human Antibodies Specific for the Third Variable Region of HIV-1 gp120 Impose Immune Pressure on Infecting Viruses. EBioMedicine. 2014;1(1):37-45.
14. Upadhyay C, Mayr LM, Zhang J, Kumar R, Gorny MK, Nadas A, et al. Distinct mechanisms regulate exposure of neutralizing epitopes in the V2 and V3 loops of HIV-1 envelope. Journal of virology. 2014;88(21):12853-65.
15. Moore PL, Gray ES, Wibmer CK, Bhiman JN, Nonyane M, Sheward DJ, et al. Evolution of an HIV glycan-dependent broadly neutralizing antibody epitope through immune escape. Nature medicine. 2012;18(11):1688-92.
16. Lynch RM, Wong P, Tran L, O'Dell S, Nason MC, Li Y, et al. HIV-1 fitness cost associated with escape from the VRC01 class of CD4 binding site neutralizing antibodies. Journal of virology. 2015;89(8):4201-13.
17. Wei X, Decker JM, Wang S, Hui H, Kappes JC, Wu X, et al. Antibody neutralization and escape by HIV-1. Nature. 2003;422(6929):307-12.

18. Doria-Rose NA, Schramm CA, Gorman J, Moore PL, Bhiman JN, DeKosky BJ, et al. Developmental pathway for potent V1V2-directed HIV-neutralizing antibodies. Nature. 2014;509(7498):55-62.
19. McLellan JS, Pancera M, Carrico C, Gorman J, Julien JP, Khayat R, et al. Structure of HIV-1 gp120 V1/V2 domain with broadly neutralizing antibody PG9. Nature. 2011;480(7377):336-43.
20. Pancera M, Shahzad-Ul-Hussan S, Doria-Rose NA, McLellan JS, Bailer RT, Dai K, et al. Structural basis for diverse N-glycan recognition by HIV-1-neutralizing V1-V2-directed antibody PG16. Nature structural & molecular biology. 2013;20(7):804-13.
21. Pejchal R, Doores KJ, Walker LM, Khayat R, Huang PS, Wang SK, et al. A potent and broad neutralizing antibody recognizes and penetrates the HIV glycan shield. Science. 2011;334(6059):1097-103.
22. Pan R, Gorny MK, Zolla-Pazner S, Kong XP. The V1V2 Region of HIV-1 gp120 Forms a Five-Stranded Beta Barrel. Journal of virology. 2015;89(15):8003-10.
23. Spurrier B, Sampson J, Gorny MK, Zolla-Pazner S, Kong XP. Functional implications of the binding mode of a human conformation-dependent V2 monoclonal antibody against HIV. Journal of virology. 2014;88(8):4100-12.
24. Liao HX, Bonsignori M, Alam SM, McLellan JS, Tomaras GD, Moody MA, et al. Vaccine induction of antibodies against a structurally heterogeneous site of immune pressure within HIV-1 envelope protein variable regions 1 and 2. Immunity. 2013;38(1):176-86.
25. van Eeden C, Wibmer CK, Scheepers C, Richardson SI, Nonyane M, Lambson B, et al. V2-Directed Vaccine-like Antibodies from HIV-1 Infection Identify an Additional K169-Binding Light Chain Motif with Broad ADCC Activity. Cell Rep. 2018;25(11):3123-35 e6.
26. Gorny MK, Pan R, Williams C, Wang XH, Volsky B, O'Neal T, et al. Functional and immunochemical cross-reactivity of V2-specific monoclonal antibodies from HIV-1-infected individuals. Virology. 2012;427(2):198-207.
27. Mayr LM, Cohen S, Spurrier B, Kong XP, Zolla-Pazner S. Epitope mapping of conformational V2-specific anti-HIV human monoclonal antibodies reveals an immunodominant site in V2. PloS one. 2013;8(7):e70859.
28. Bonsignori M, Hwang KK, Chen X, Tsao CY, Morris L, Gray E, et al. Analysis of a clonal lineage of HIV-1 envelope V2/V3 conformational epitope-specific broadly neutralizing antibodies and their inferred unmutated common ancestors. Journal of virology. 2011;85(19):9998-10009.
29. Walker LM, Phogat SK, Chan-Hui PY, Wagner D, Phung P, Goss JL, et al. Broad and potent neutralizing antibodies from an African donor reveal a new HIV-1 vaccine target. Science. 2009;326(5950):285-9.
30. Doores KJ, Kong L, Krumm SA, Le KM, Sok D, Laserson U, et al. Two classes of broadly neutralizing antibodies within a single lineage directed to the high-mannose patch of HIV envelope. Journal of virology. 2015;89(2):1105-18.
31. Scanlan CN, Pantophlet R, Wormald MR, Ollmann Saphire E, Stanfield R, Wilson IA, et al. The broadly neutralizing anti-human immunodeficiency virus type 1 antibody 2G12 recognizes a cluster of alpha1-->2 mannose residues on the outer face of gp120. Journal of virology. 2002;76(14):7306-21.
32. Pritchard LK, Spencer DI, Royle L, Bonomelli C, Seabright GE, Behrens AJ, et al. Glycan clustering stabilizes the mannose patch of HIV-1 and preserves vulnerability to broadly neutralizing antibodies. Nat Commun. 2015;6:7479.
33. Doores KJ, Bonomelli C, Harvey DJ, Vasiljevic S, Dwek RA, Burton DR, et al. Envelope glycans of immunodeficiency virions are almost entirely oligomannose antigens. Proceedings of the National Academy of Sciences of the United States of America. 2010;107(31):13800-5.

34. Upadhyay C, Feyznezhad R, Yang W, Zhang H, Zolla-Pazner S, Hioe CE. Alterations of HIV-1 envelope phenotype and antibody-mediated neutralization by signal peptide mutations. PLoS pathogens. 2018;14(1):e1006812.
35. Yolitz J, Schwing C, Chang J, Van Ryk D, Nawaz F, Wei D, et al. Signal peptide of HIV envelope protein impacts glycosylation and antigenicity of gp120. Proceedings of the National Academy of Sciences of the United States of America. 2018;115(10):2443-8.
36. da Silva JX, Franco OL, Lemos MA, Gondim MV, Prosdocimi F, Arganaraz ER. Sequence variations of Env signal peptide alleles in different clinical stages of HIV infection. Peptides. 2011;32(9):1800-6.
37. Asmal M, Hellmann I, Liu W, Keele BF, Perelson AS, Bhattacharya T, et al. A signature in HIV-1 envelope leader peptide associated with transition from acute to chronic infection impacts envelope processing and infectivity. PloS one. 2011;6(8):e23673.
38. AlSalmi W, Mahalingam M, Ananthaswamy N, Hamlin C, Flores D, Gao G, et al. A New Approach to Produce HIV-1 Envelope Trimers: BOTH CLEAVAGE AND PROPER GLYCOSYLATION ARE ESSENTIAL TO GENERATE AUTHENTIC TRIMERS. J Biol Chem. 2015;290(32):19780-95.
39. Sanders RW, Derking R, Cupo A, Julien JP, Yasmeen A, de Val N, et al. A next-generation cleaved, soluble HIV-1 Env trimer, BG505 SOSIP.664 gp140, expresses multiple epitopes for broadly neutralizing but not non-neutralizing antibodies. PLoS pathogens. 2013;9(9):e1003618.
40. Alam SM, Liao HX, Tomaras GD, Bonsignori M, Tsao CY, Hwang KK, et al. Antigenicity and immunogenicity of RV144 vaccine AIDSVAX clade E envelope immunogen is enhanced by a gp120 N-terminal deletion. Journal of virology. 2013;87(3):1554-68.
41. Lasky LA, Groopman JE, Fennie CW, Benz PM, Capon DJ, Dowbenko DJ, et al. Neutralization of the AIDS retrovirus by antibodies to a recombinant envelope glycoprotein. Science. 1986;233(4760):209-12.
42. Berman PW. Development of bivalent rgp120 vaccines to prevent HIV type 1 infection. AIDS Res Hum Retroviruses. 1998;14 Suppl 3:S277-89.
43. Land A, Zonneveld D, Braakman I. Folding of HIV-1 envelope glycoprotein involves extensive isomerization of disulfide bonds and conformation-dependent leader peptide cleavage. FASEB J. 2003;17(9):1058-67.
44. von Heijne G. Signal sequences. The limits of variation. Journal of molecular biology. 1985;184(1):99-105.
45. von Heijne G, Gavel Y. Topogenic signals in integral membrane proteins. Eur J Biochem. 1988;174(4):671-8.
46. Arnold A, Horst SA, Gardella TJ, Baba H, Levine MA, Kronenberg HM. Mutation of the signal peptide-encoding region of the preproparathyroid hormone gene in familial isolated hypoparathyroidism. J Clin Invest. 1990;86(4):1084-7.
47. Schiemann WP, Rotzer D, Pfeifer WM, Levi E, Rai KR, Knaus P, et al. Transforming growth factor-beta (TGF-beta)-resistant B cells from chronic lymphocytic leukemia patients contain recurrent mutations in the signal sequence of the type I TGF-beta receptor. Cancer Detect Prev. 2004;28(1):57-64.
48. Meur G, Simon A, Harun N, Virally M, Dechaume A, Bonnefond A, et al. Insulin gene mutations resulting in early-onset diabetes: marked differences in clinical presentation, metabolic status, and pathogenic effect through endoplasmic reticulum retention. Diabetes. 2010;59(3):653-61.
49. Piersma D, Berns EM, Verhoef-Post M, Uitterlinden AG, Braakman I, Pols HA, et al. A common polymorphism renders the luteinizing hormone receptor protein more active by improving signal peptide function and predicts adverse outcome in breast cancer patients. J Clin Endocrinol Metab. 2006;91(4):1470-6.

50. Ding B, Kull B, Liu Z, Mottagui-Tabar S, Thonberg H, Gu HF, et al. Human neuropeptide Y signal peptide gain-of-function polymorphism is associated with increased body mass index: possible mode of function. Regul Pept. 2005;127(1-3):45-53.
51. Witt H, Luck W, Becker M. A signal peptide cleavage site mutation in the cationic trypsinogen gene is strongly associated with chronic pancreatitis. Gastroenterology. 1999;117(1):7-10.
52. Jan M, Upadhyay C, Alcami Pertejo J, Hioe CE, Arora SK. Heterogeneity in glycan composition on the surface of HIV-1 envelope determines virus sensitivity to lectins. PloS one. 2018;13(3):e0194498.
53. Lindemann D, Pietschmann T, Picard-Maureau M, Berg A, Heinkelein M, Thurow J, et al. A particle-associated glycoprotein signal peptide essential for virus maturation and infectivity. Journal of virology. 2001;75(13):5762-71.
54. Feldman D, Roniger M, Bar-Sinai A, Braitbard O, Natan C, Love DC, et al. The signal peptide of mouse mammary tumor virus-env: a phosphoprotein tumor modulator. Mol Cancer Res. 2012;10(8):1077-86.
55. Seaman MS, Janes H, Hawkins N, Grandpre LE, Devoy C, Giri A, et al. Tiered categorization of a diverse panel of HIV-1 Env pseudoviruses for assessment of neutralizing antibodies. Journal of virology. 2010;84(3):1439-52.
56. deCamp A, Hraber P, Bailer RT, Seaman MS, Ochsenbauer C, Kappes J, et al. Global panel of HIV-1 Env reference strains for standardized assessments of vaccine-elicited neutralizing antibodies. Journal of virology. 2014;88(5):2489-507.
57. Olausson J, Tibell L, Jonsson BH, Pahlsson P. Detection of a high affinity binding site in recombinant Aleuria aurantia lectin. Glycoconj J. 2008;25(8):753-62.
58. Hester G, Kaku H, Goldstein IJ, Wright CS. Structure of mannose-specific snowdrop (Galanthus nivalis) lectin is representative of a new plant lectin family. Nat Struct Biol. 1995;2(6):472-9.
59. Sok D, Pauthner M, Briney B, Lee JH, Saye-Francisco KL, Hsueh J, et al. A Prominent Site of Antibody Vulnerability on HIV Envelope Incorporates a Motif Associated with CCR5 Binding and Its Camouflaging Glycans. Immunity. 2016;45(1):31-45.
60. Rantalainen K, Berndsen ZT, Murrell S, Cao L, Omorodion O, Torres JL, et al. Co-evolution of HIV Envelope and Apex-Targeting Neutralizing Antibody Lineage Provides Benchmarks for Vaccine Design. Cell Rep. 2018;23(11):3249-61.
61. Doores KJ, Burton DR. Variable loop glycan dependency of the broad and potent HIV-1-neutralizing antibodies PG9 and PG16. Journal of virology. 2010;84(20):10510-21.
62. Go EP, Liao HX, Alam SM, Hua D, Haynes BF, Desaire H. Characterization of host-cell line specific glycosylation profiles of early transmitted/founder HIV-1 gp120 envelope proteins. J Proteome Res. 2013;12(3):1223-34.
63. Raska M, Takahashi K, Czernekova L, Zachova K, Hall S, Moldoveanu Z, et al. Glycosylation patterns of HIV-1 gp120 depend on the type of expressing cells and affect antibody recognition. J Biol Chem. 2010;285(27):20860-9.
64. Behrens AJ, Vasiljevic S, Pritchard LK, Harvey DJ, Andev RS, Krumm SA, et al. Composition and Antigenic Effects of Individual Glycan Sites of a Trimeric HIV-1 Envelope Glycoprotein. Cell Rep. 2016;14(11):2695-706.
65. Shivatare VS, Shivatare SS, Lee CD, Liang CH, Liao KS, Cheng YY, et al. Unprecedented Role of Hybrid N-Glycans as Ligands for HIV-1 Broadly Neutralizing Antibodies. J Am Chem Soc. 2018;140(15):5202-10.
66. O'Rourke SM, Sutthent R, Phung P, Mesa KA, Frigon NL, To B, et al. Glycans flanking the hypervariable connecting peptide between the A and B strands of the V1/V2 domain of HIV-1 gp120 confer resistance to antibodies that neutralize CRF01_AE viruses. PloS one. 2015;10(3):e0119608.

67. Behrens AJ, Harvey DJ, Milne E, Cupo A, Kumar A, Zitzmann N, et al. Molecular Architecture of the Cleavage-Dependent Mannose Patch on a Soluble HIV-1 Envelope Glycoprotein Trimer. Journal of virology. 2017;91(2).
68. Pritchard LK, Vasiljevic S, Ozorowski G, Seabright GE, Cupo A, Ringe R, et al. Structural Constraints Determine the Glycosylation of HIV-1 Envelope Trimers. Cell Rep. 2015;11(10):1604-13.
69. Struwe WB, Chertova E, Allen JD, Seabright GE, Watanabe Y, Harvey DJ, et al. Site-Specific Glycosylation of Virion-Derived HIV-1 Env Is Mimicked by a Soluble Trimeric Immunogen. Cell Rep. 2018;24(8):1958-66 e5.
70. Ringe RP, Ozorowski G, Yasmeen A, Cupo A, Cruz Portillo VM, Pugach P, et al. Improving the Expression and Purification of Soluble, Recombinant Native-Like HIV-1 Envelope Glycoprotein Trimers by Targeted Sequence Changes. Journal of virology. 2017;91(12).
71. Blattner C, Lee JH, Sliepen K, Derking R, Falkowska E, de la Pena AT, et al. Structural delineation of a quaternary, cleavage-dependent epitope at the gp41-gp120 interface on intact HIV-1 Env trimers. Immunity. 2014;40(5):669-80.
72. Han Q, Jones JA, Nicely NI, Reed RK, Shen X, Mansouri K, et al. Difficult-to-neutralize global HIV-1 isolates are neutralized by antibodies targeting open envelope conformations. Nat Commun. 2019;10(1):2898.
73. Zolla-Pazner S, Cohen SS, Boyd D, Kong XP, Seaman M, Nussenzweig M, et al. Structure/Function Studies Involving the V3 Region of the HIV-1 Envelope Delineate Multiple Factors That Affect Neutralization Sensitivity. Journal of virology. 2016;90(2):636-49.
74. de Taeye SW, de la Pena AT, Vecchione A, Scutigliani E, Sliepen K, Burger JA, et al. Stabilization of the gp120 V3 loop through hydrophobic interactions reduces the immunodominant V3-directed non-neutralizing response to HIV-1 envelope trimers. J Biol Chem. 2018;293(5):1688-701.
75. Hogan MJ, Conde-Motter A, Jordan APO, Yang L, Cleveland B, Guo W, et al. Increased surface expression of HIV-1 envelope is associated with improved antibody response in vaccinia prime/protein boost immunization. Virology. 2018;514:106-17.
76. Rutkowski DT, Ott CM, Polansky JR, Lingappa VR. Signal sequences initiate the pathway of maturation in the endoplasmic reticulum lumen. J Biol Chem. 2003;278(32):30365-72.
77. Martoglio B, Dobberstein B. Signal sequences: more than just greasy peptides. Trends in cell biology. 1998;8(10):410-5.
78. Nielsen H, Engelbrecht J, Brunak S, von Heijne G. Identification of prokaryotic and eukaryotic signal peptides and prediction of their cleavage sites. Protein Eng. 1997;10(1):1-6.
79. Buchan DW, Ward SM, Lobley AE, Nugent TC, Bryson K, Jones DT. Protein annotation and modelling servers at University College London. Nucleic Acids Res. 2010;38(Web Server issue):W563-8.
80. Buchan DWA, Jones DT. The PSIPRED Protein Analysis Workbench: 20 years on. Nucleic Acids Res. 2019;47(W1):W402-W7.
81. Wang JY, Song WT, Li Y, Chen WJ, Yang D, Zhong GC, et al. Improved expression of secretory and trimeric proteins in mammalian cells via the introduction of a new trimer motif and a mutant of the tPA signal sequence. Appl Microbiol Biotechnol. 2011;91(3):731-40.
82. Nilsson I, Lara P, Hessa T, Johnson AE, von Heijne G, Karamyshev AL. The code for directing proteins for translocation across ER membrane: SRP cotranslationally recognizes specific features of a signal sequence. Journal of molecular biology. 2015;427(6 Pt A):1191-201.
83. Peterson JH, Woolhead CA, Bernstein HD. Basic amino acids in a distinct subset of signal peptides promote interaction with the signal recognition particle. J Biol Chem. 2003;278(46):46155-62.

84. Walter P, Ibrahimi I, Blobel G. Translocation of proteins across the endoplasmic reticulum. I. Signal recognition protein (SRP) binds to in-vitro-assembled polysomes synthesizing secretory protein. J Cell Biol. 1981;91(2 Pt 1):545-50.
85. Earl PL, Moss B, Doms RW. Folding, interaction with GRP78-BiP, assembly, and transport of the human immunodeficiency virus type 1 envelope protein. Journal of virology. 1991;65(4):2047-55.
86. Zheng N, Gierasch LM. Signal sequences: the same yet different. Cell. 1996;86(6):849-52.
87. Adams H, Scotti PA, De Cock H, Luirink J, Tommassen J. The presence of a helix breaker in the hydrophobic core of signal sequences of secretory proteins prevents recognition by the signal-recognition particle in Escherichia coli. Eur J Biochem. 2002;269(22):5564-71.
88. Keenan RJ, Freymann DM, Walter P, Stroud RM. Crystal structure of the signal sequence binding subunit of the signal recognition particle. Cell. 1998;94(2):181-91.
89. Martoglio B, Graf R, Dobberstein B. Signal peptide fragments of preprolactin and HIV-1 p-gp160 interact with calmodulin. EMBO J. 1997;16(22):6636-45.
90. Li M, Gao F, Mascola JR, Stamatatos L, Polonis VR, Koutsoukos M, et al. Human immunodeficiency virus type 1 env clones from acute and early subtype B infections for standardized assessments of vaccine-elicited neutralizing antibodies. Journal of virology. 2005;79(16):10108-25.
91. Gorny MK, Moore JP, Conley AJ, Karwowska S, Sodroski J, Williams C, et al. Human anti-V2 monoclonal antibody that neutralizes primary but not laboratory isolates of human immunodeficiency virus type 1. Journal of virology. 1994;68(12):8312-20.
92. Nyambi PN, Mbah HA, Burda S, Williams C, Gorny MK, Nadas A, et al. Conserved and exposed epitopes on intact, native, primary human immunodeficiency virus type 1 virions of group M. Journal of virology. 2000;74(15):7096-107.
93. Pinter A, Honnen WJ, He Y, Gorny MK, Zolla-Pazner S, Kayman SC. The V1/V2 domain of gp120 is a global regulator of the sensitivity of primary human immunodeficiency virus type 1 isolates to neutralization by antibodies commonly induced upon infection. Journal of virology. 2004;78(10):5205-15.
94. Gorny MK, Conley AJ, Karwowska S, Buchbinder A, Xu JY, Emini EA, et al. Neutralization of diverse human immunodeficiency virus type 1 variants by an anti-V3 human monoclonal antibody. Journal of virology. 1992;66(12):7538-42.
95. Gorny MK, Williams C, Volsky B, Revesz K, Wang XH, Burda S, et al. Cross-clade neutralizing activity of human anti-V3 monoclonal antibodies derived from the cells of individuals infected with non-B clades of human immunodeficiency virus type 1. Journal of virology. 2006;80(14):6865-72.
96. Hioe CE, Wrin T, Seaman MS, Yu X, Wood B, Self S, et al. Anti-V3 monoclonal antibodies display broad neutralizing activities against multiple HIV-1 subtypes. PloS one. 2010;5(4):e10254.
97. Gigler A, Dorsch S, Hemauer A, Williams C, Kim S, Young NS, et al. Generation of neutralizing human monoclonal antibodies against parvovirus B19 proteins. Journal of virology. 1999;73(3):1974-9.
98. Montefiori DC. Evaluating neutralizing antibodies against HIV, SIV, and SHIV in luciferase reporter gene assays. Current protocols in immunology. 2005;Chapter 12:Unit 12 1.
99. Altman JB, Liu X, Itri V, Zolla-Pazner S, Powell RLR. Optimized protocol for detection of native, full-length HIV-1 envelope on the surface of transfected cells. Health Sci Rep. 2018;1(9):e74.
100. Cao L, Diedrich JK, Kulp DW, Pauthner M, He L, Park SR, et al. Global site-specific N-glycosylation analysis of HIV envelope glycoprotein. Nat Commun. 2017;8:14954.
101. Angel PM, Lim JM, Wells L, Bergmann C, Orlando R. A potential pitfall in 18O-based N-linked glycosylation site mapping. Rapid Commun Mass Spectrom. 2007;21(5):674-82.

102. Kaji H, Saito H, Yamauchi Y, Shinkawa T, Taoka M, Hirabayashi J, et al. Lectin affinity capture, isotope-coded tagging and mass spectrometry to identify N-linked glycoproteins. Nature biotechnology. 2003;21(6):667-72.

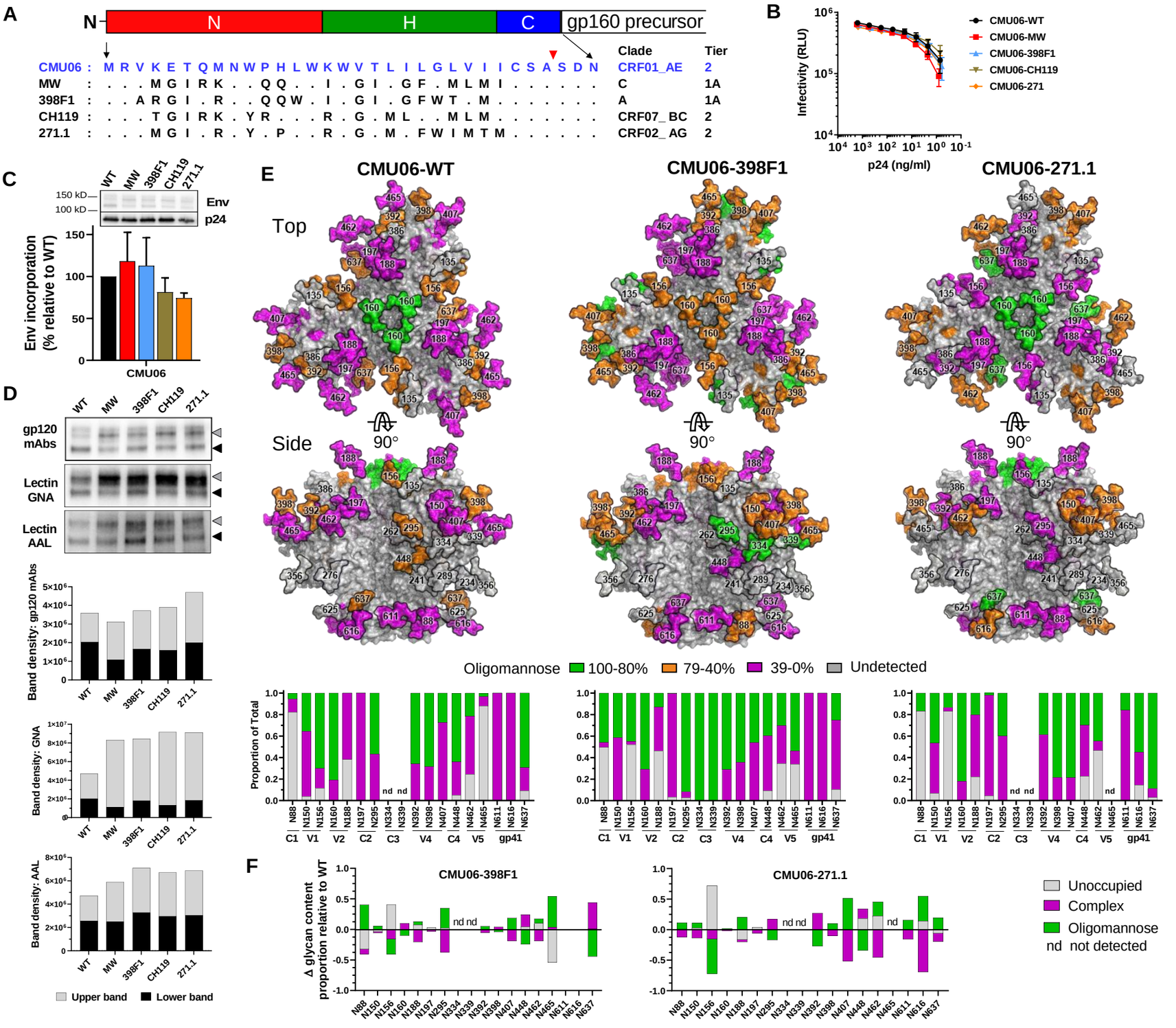

Fig. 1: Effect of SP swap on CMU06 Env glycosylation. (A) CMU06 WT and swapped SPs. SP cleavage site is denoted by red triangle. (B) Infectivity of WT vs SP-swapped CMU06 in CD4+ TZM.bl cells. Viruses were produced in 293T cells. (C) Measurement of WT vs SP-swapped Env incorporation into CMU06 virions produced in 293T cells by Western blot. A gp120 mAb cocktail and a p24 Gag mAb were used. Levels of Env incorporation were based on Env/p24 ratios (WT=100%). **(D)** Assessment of Env glycan content by lectin-probed Western blotting. Comparable amounts of Envs from 293T-produced sucrose-pelleted virions were separated by SDS-PAGE, blotted, and probed with a gp120 mAb cocktail or lectins (GNA and AAL). Density of upper and lower Env bands (grey and black arrows) were measured. **(E)** Top panel: Env trimer models (generated using a SOSIP.664 trimer PDB 5FYJ) showing the predominating glycoforms at each of the CMU06 glycosites for CMU06-WT, CMU06-398F1, and CMU06-271.1. Type of glycans added was based on LC-MS/MS data of virion-associated Envs from 293T cells (bar graphs, bottom panel). Bottom panel: Relative amounts of unoccupied, oligomannose, and complex glycans at glycosites on SP-swapped vs WT CMU06 as determined by LC-MS/MS. nd: glycosites not detected in 1 or 2 Envs. **(F)** Changes in glycan content at each glycosite for CMU06-398F1 and CMU06-271.1 vs CMU06-WT calculated from Figure 1E data.

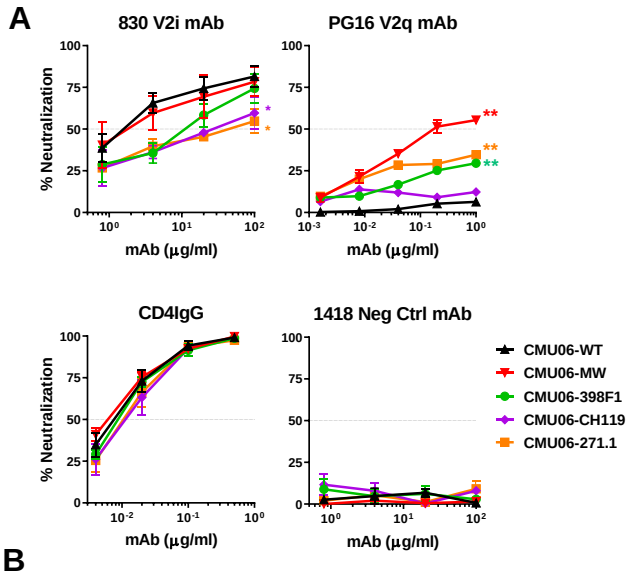

B

Env epitope	mAbs	CMU06 Neutralization (AUC)				
		WT	MW	398F1	CH119	271
V1V2	697	63	52	53	37	32
	830	140	132	102	89	88
	1357	33	35	29	25	25
	1361	79	66	68	56	45
	1393	87	81	81	61	52
	2158	96	87	78	58	67
V2p	CH59	162	194	173	173	179
V2q	PG9	127	168	166	139	158
	PG16	20	158	86	47	115
V3	2219	13	36	9	3	10
	2557	16	56	34	21	20
CD4bs	NIH45-46	206	215	178	186	194
	VRC01	121	143	128	112	116
	3BNC117	166	186	176	167	185
gp41	2F5	64	71	54	74	66
CD4-IgG		164	166	159	153	155
non-HIV	1418	9	2	12	13	8

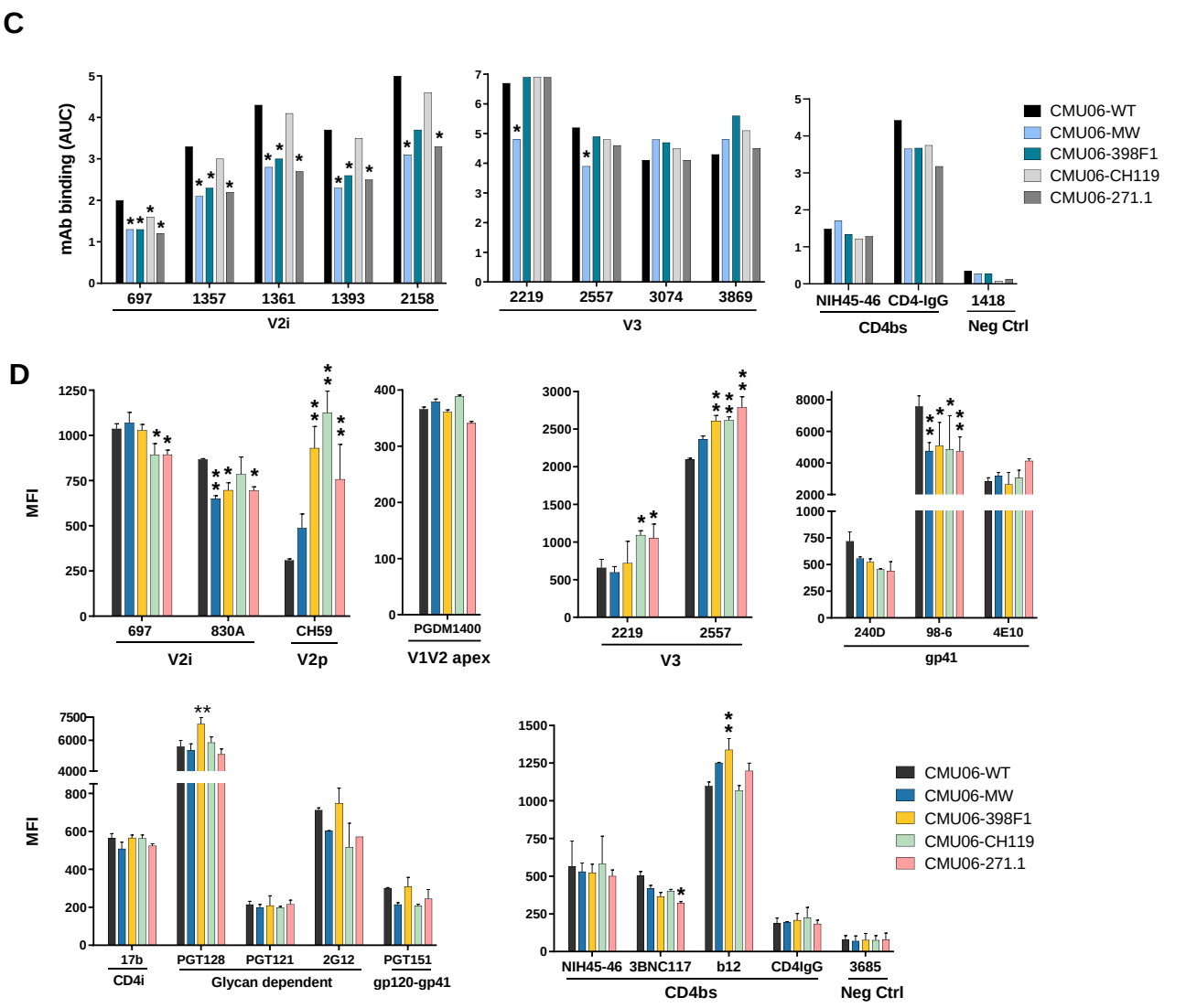

Fig. 2: Effect of SP swap on CMU06 Env-antibody interaction. (A) Neutralization of 293T-derived CMU06. Viruses were incubated with titrated mAbs at 37°C for 24 hours before addition of TZM.bl cells, except for PG9, NIH45-46, VRC01, 3BNC117, 2F5 and CD4-IgG which were pre-incubated with viruses for 1 hour. MAb 1418 served as negative control. Representative neutralization curves are shown. Mean and SEM from 2-3 experiments are shown. **(B)** Neutralization AUCs (areas under the curves) of WT vs SP-swapped CMU06 with different mAbs. Decrease and increase in AUC values by >30% and p<0.05 are shown in red and blue respectively. **(C)** ELISA binding of mAbs to gp120 derived from CMU06-WT vs SP-swapped viruses. MAbs were titrated ten-fold from 10 µg/ml, while CD4-IgG was titrated five-fold from 10 µg/ml. AUC values are shown. **(D)** Binding of mAbs to WT vs SP-swapped Envs expressed on the surface of 293T cells. MAbs were tested at following concentrations: 697, 830 and 3685 at 100µg/ml; 2G12 at 50µg/ml; PGDM1400, 2219, 2557, 240D, 98-6 and PGT121 at 25µg/ml; b12 at 20µg/ml; 4E10, 17b at 10µg/ml; PGT128, PGT151, 3BNC117 and CD4-IgG at 5µg/ml; CH59 and NIH45-46 at 2.5µg/ml. Geometric mean fluorescence intensity (MFI) and SD from duplicates in one experiment are shown. Data were analyzed by 2-way ANOVA (* $p < 0.05$, ** $p < 0.01$, vs WT).

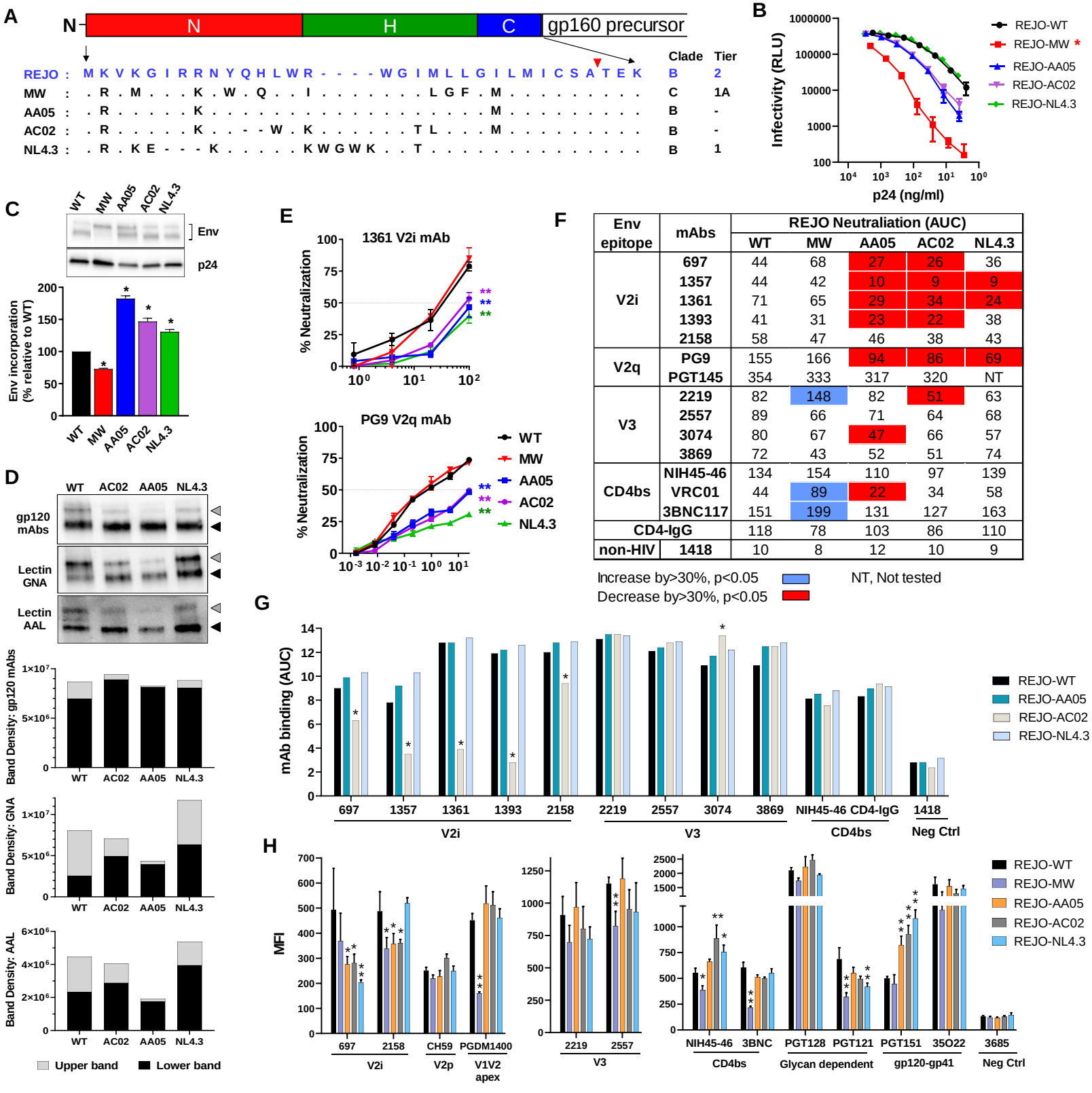

Env epitope	mAbs	REJO Neutraliation (AUC)				
		WT	MW	AA05	AC02	NL4.3
V2i	697	44	68	27	26	36
	1357	44	42	10	9	9
	1361	71	65	29	34	24
	1393	41	31	23	22	38
	2158	58	47	46	38	43
V2q	PG9	155	166	94	86	69
	PGT145	354	333	317	320	NT
V3	2219	82	148	82	51	63
	2557	89	66	71	64	68
	3074	80	67	47	66	57
	3869	72	43	52	51	74
CD4bs	NIH45-46	134	154	110	97	139
	VRC01	44	89	22	34	58
	3BNC117	151	199	131	127	163
CD4-IgG		118	78	103	86	110
non-HIV	1418	10	8	12	10	9

Fig. 3: Effects of SP swap on REJO. (A) REJO WT and swapped SPs. Red triangle: SP cleavage site. -, undetermined. **(B)** Infectivity of WT vs SP-swapped REJO from 293T cells in TZM.bl cells. *, p = 0.01 vs WT by Mann-Whitney test. **(C)** Measurement of Env incorporation into virions by Western blot as in Fig 1C. *, p≤ 0.005 vs WT by unpaired t-test. **(D)** Analysis of REJO Env glycosylation by lectin-probed Western blotting as in Fig 1d. **(E)** Neutralization of WT and SP-swapped REJO treated with titrated amounts of anti-Env mAbs. Neutralization was performed as in Fig 2A-B. Data for V2i mAb 1361 and V2q mAb PG9 are shown. **, p< 0.001 vs WT by 2-way ANOVA. **(F)** Neutralization AUCs of WT vs SP-swapped viruses with different mAbs. NT, not tested. **(G)** ELISA binding of mAbs and CD4-IgG to gp120 from WT and SP-swapped viruses. Titration was done as in Fig 2D and AUCs are shown. *, p< 0.05 vs WT by ANOVA of the titration curves. **(H)** Binding of mAbs to REJO WT vs SP-swapped Envs expressed on the surface of 293T cells. MAbs were tested at concentration: 697, 2158 and 3685 at 100µg/ml; 2219 and 2557 at 50µg/ml; PGT128 and PGT121 at 25 µg/ml; CH59, 3BNC117 at 20µg/ml; PGDM1400 and PGT151 at 10µg/ml; NIH45-46 at 2.5µg/ml. Averages and SEM of MFI from duplicates of two experiments are shown. *, p< 0.05; ** p< 0.01 vs WT by 2-way ANOVA.

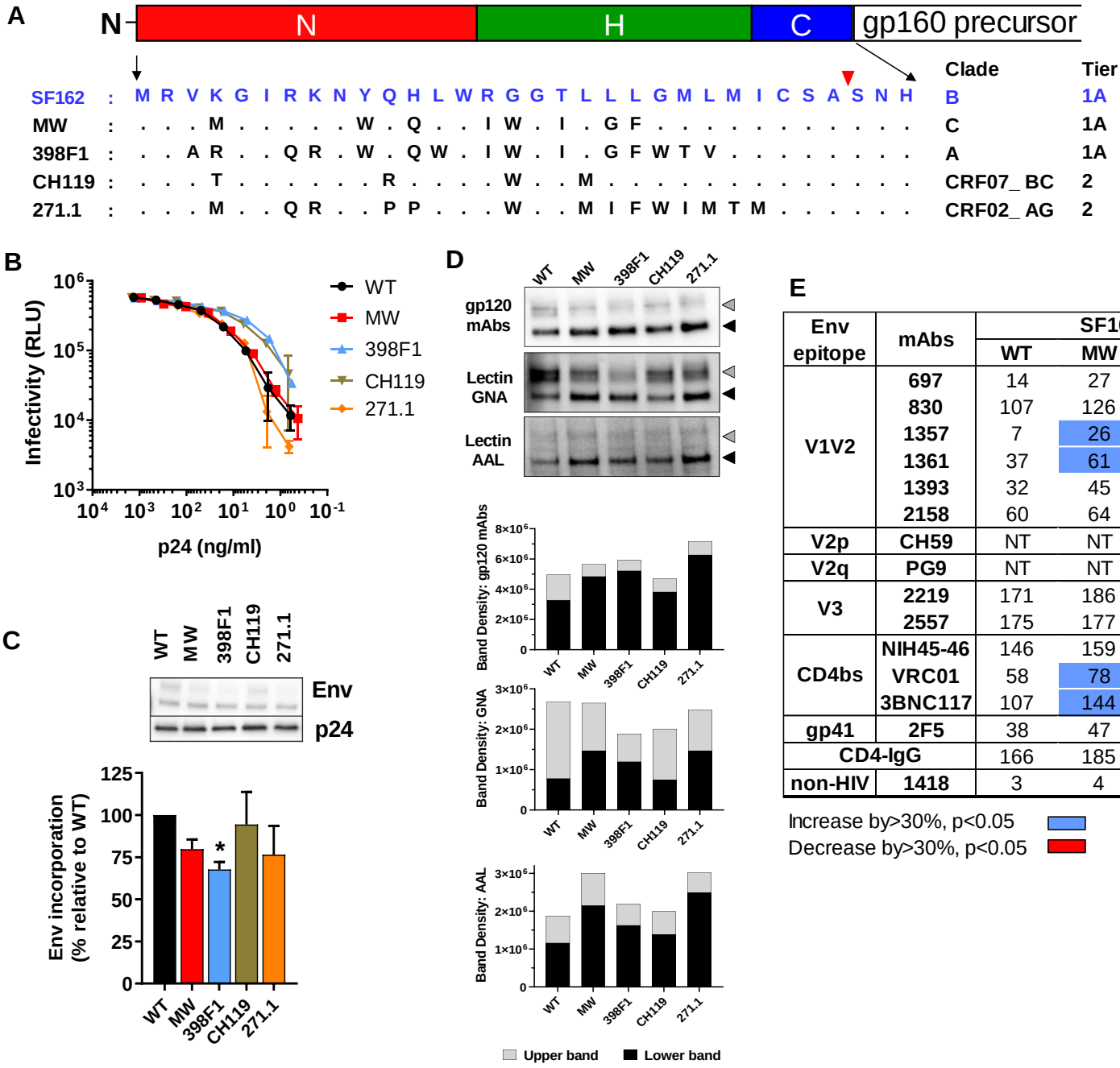

Env epitope	mAbs	SF162 Viruses: 293T				
		WT	MW	398F1	CH119	271
V1V2	697	14	27	27	18	22
	830	107	126	106	121	115
	1357	7	26	11	6	15
	1361	37	61	48	37	48
	1393	32	45	35	36	41
	2158	60	64	73	58	60
V2p	CH59	NT	NT	NT	NT	NT
V2q	PG9	NT	NT	NT	NT	NT
V3	2219	171	186	176	180	185
	2557	175	177	172	177	170
CD4bs	NIH45-46	146	159	170	166	160
	VRC01	58	78	74	70	86
	3BNC117	107	144	157	126	126
gp41	2F5	38	47	19	26	33
CD4-IgG		166	185	185	169	171
non-HIV	1418	3	4	4	3	2

Increase by>30%, p<0.05
Decrease by>30%, p<0.05
NT, Not tested

Fig. 4: Effect of SP swap on SF162. (A) SF162-WT and swapped SPs. Red triangle: SP cleavage site. **(B)** Infectivity of 293T-derived SF162 WT vs SP-swapped viruses in TZM.bl cells. **(C)** Measurement of Env incorporation by Western blot as in Fig 1C. *, p = 0.017 vs WT by unpaired t-test. **(D)** Binding of Env from SF162 WT and SP-swapped viruses by gp120 mAbs and lectins (GNA and AAL) in Western blots. Densities of upper and lower Env bands (gray and black arrows) are shown. **(E)** Neutralization AUCs of WT vs SP-swapped viruses with different mAbs.

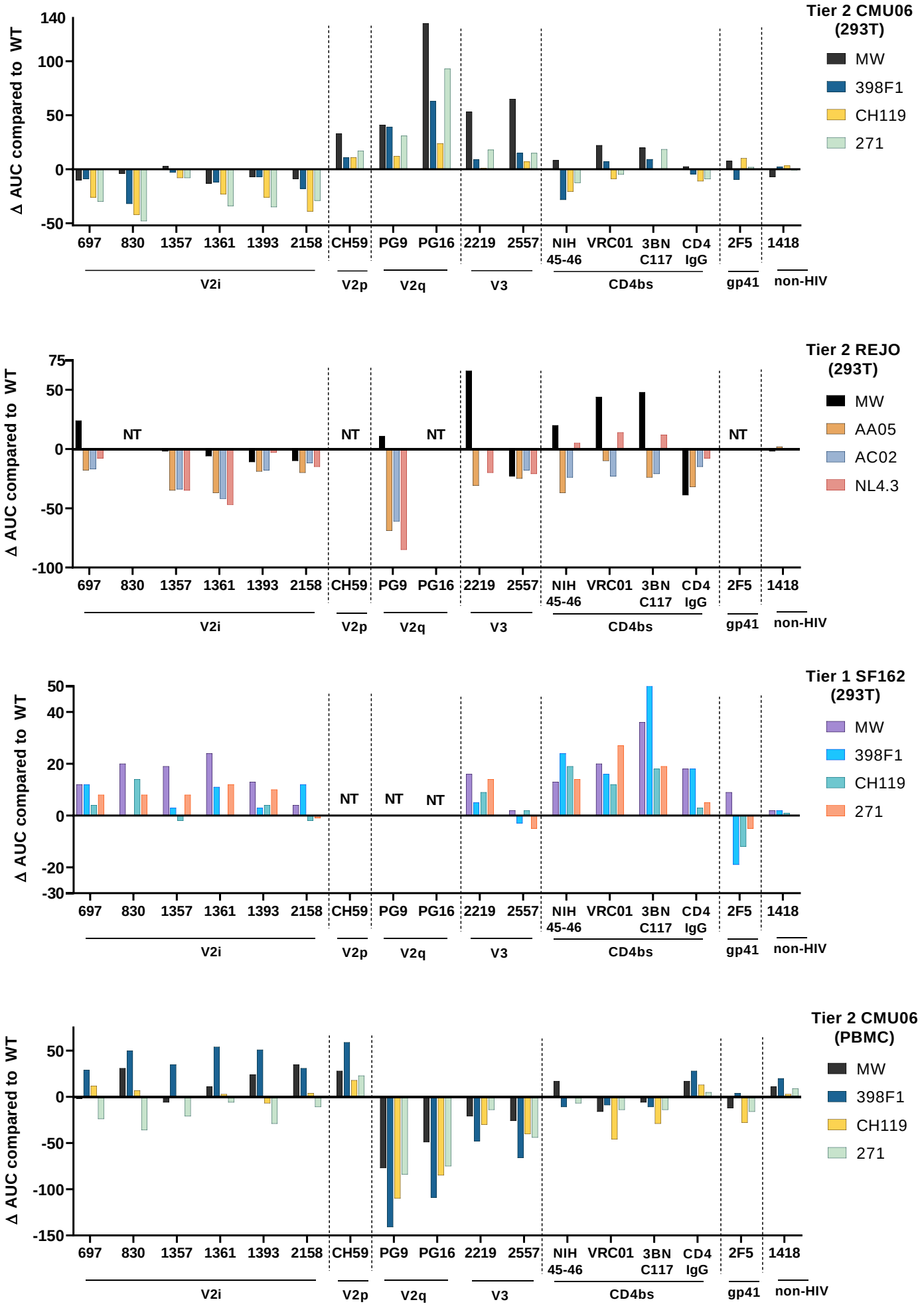

Fig. 5: Changes of neutralization sensitivity in the context of different Envs and SPs. AUC changes relative to the respective WT were calculated: (SP-swapped AUC – WT AUC). NT, not tested.

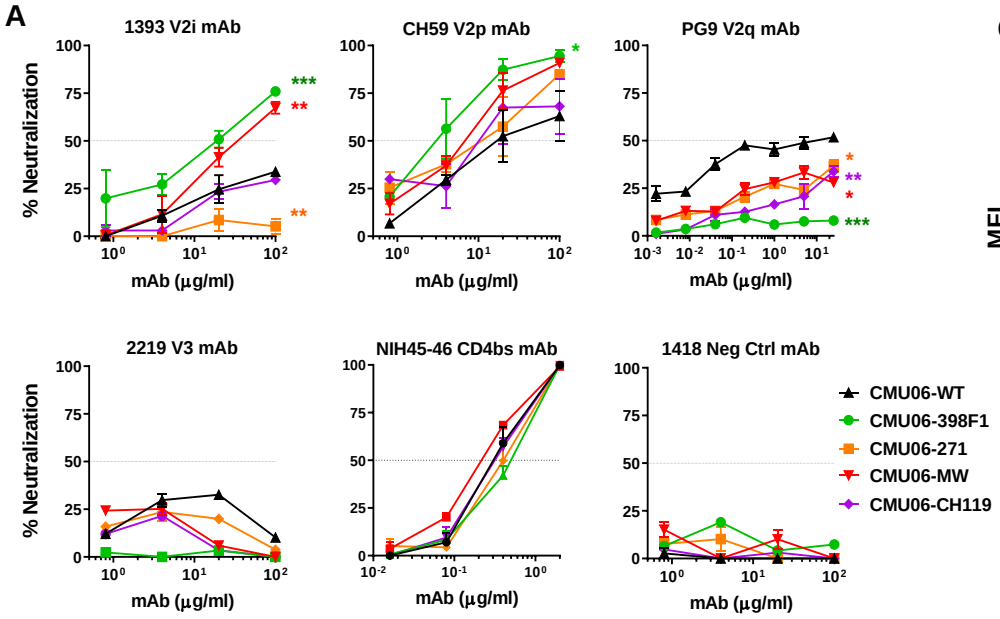

B

Env epitope	mAbs	CMU06 Neutralization (AUC)				
		WT	MW	398F1	CH119	271
V1V2	697	49	47	78	61	24
	830	73	104	123	79	37
	1357	32	26	67	32	11
	1361	15	26	70	19	10
	1393	37	61	88	30	8
	2158	47	83	78	52	37
V2p	CH59	82	110	141	100	105
V2q	PG9	168	91	26	57	83
	PG16	123	73	14	37	48
V3	2219	51	30	3	22	37
	2557	75	48	9	35	31
CD4bs	NIH45-46	81	98	70	81	74
	VRC01	83	67	74	37	69
	3BNC117	119	114	108	90	106
gp41	2F5	48	36	52	20	31
CD4-Ig		102	119	130	115	107
non-HIV	1418	1	12	21	4	10

Decrease by>30%, p<0.05

Increase by >30%, p<0.05

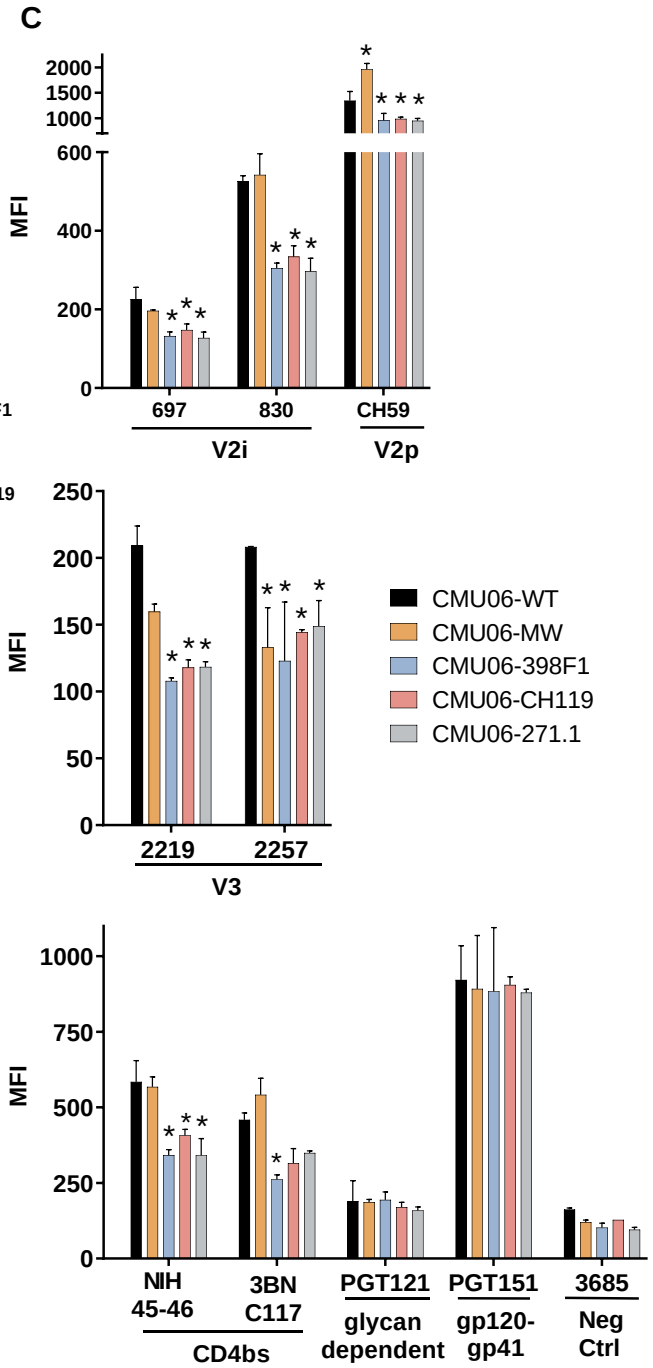

Fig. 6: Effect of SP swap on neutralization of CMU06 produced in PBMCs and antigenicity of CMU06 Env expressed on human CD4⁺ T cells. (A) Virus neutralization was measured using TZM.bl cells. MAb 1418 served as a negative control. Neutralization curves of selected virus-mAb pairs are shown. *, $p < 0.05$, **, $p < 0.01$, ***, $p < 0.001$, vs WT by 2-way ANOVA. **(B)** Neutralization AUCs of WT vs SP-swapped viruses by different mAbs. **(C)** Binding of mAbs to Env expressed on CD4⁺ T cell surface. MAbs were tested at the concentrations: 697, 830, 2219 and 2557 and 3685 at 100µg/ml; PGT121 25µg/ml; CH59 and PGT151 at 10µg/ml; NIH45-46 at 2.5µg/ml; 3BNC117 at 20µg/ml. MFI and SD from duplicates of one experiment are shown. *, $p< 0.05$ vs WT by ANOVA.

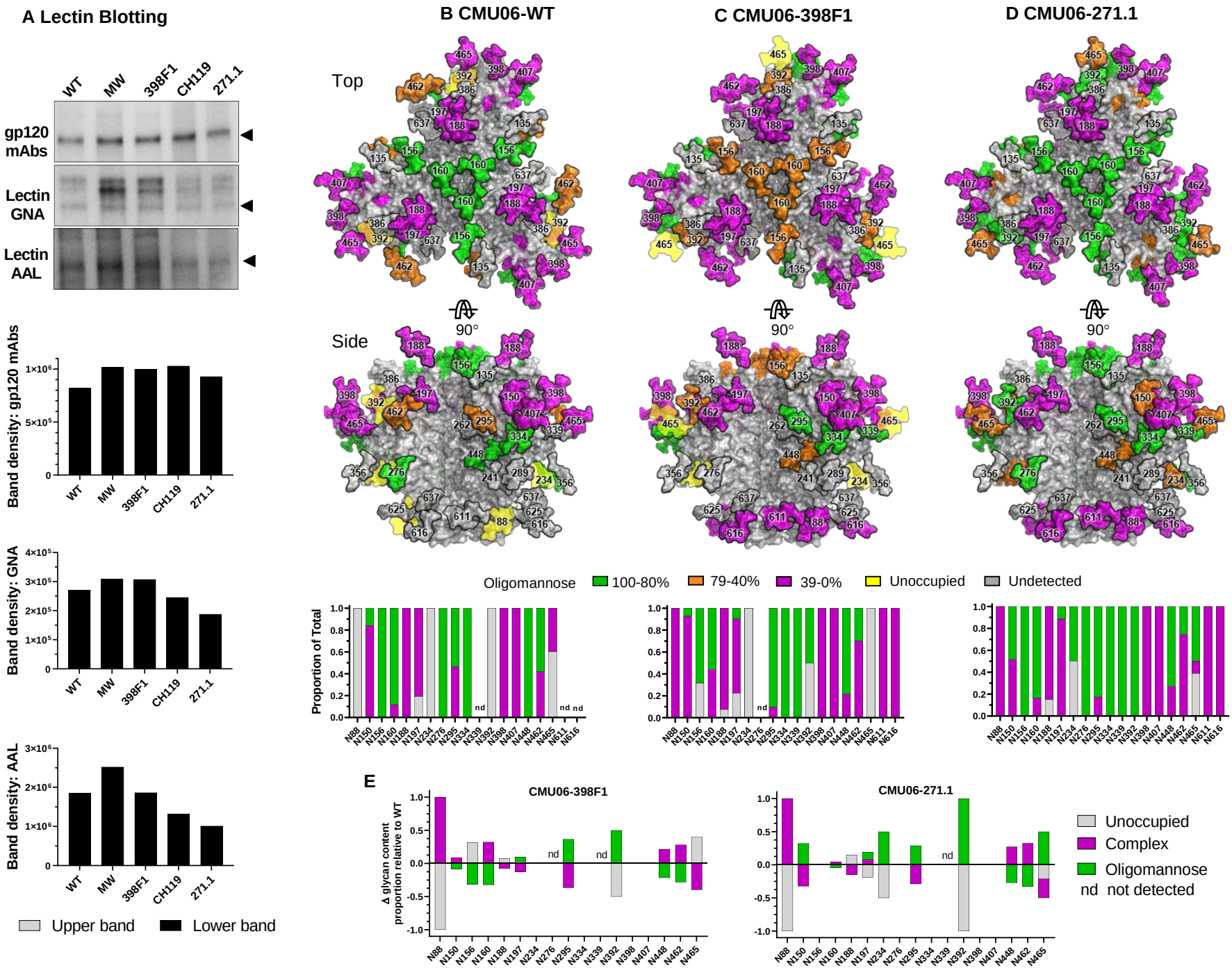

Fig. 7: Changes in glycosylation on Env of CMU06 WT and SP-swapped viruses produced in PBMC. (A) Binding of Env by mAbs and lectins (GNA and AAL) measured in Western blots. **(B-D)** Top panel: Models of glycosylated Env trimers from PBMC-derived CMU06 WT and SP-swapped viruses. Models and glycans were generated as in Fig 1E. Bottom panel: Proportions of unoccupied, oligomannose, and complex glycans at each glycosite. **(E)** Changes in glycan content at each glycosite for CMU06-398F1 and CMU06-271.1 vs CMU06-WT calculated from data in fig 7B-D bottom panels. Glycosites undetected in all 3 Envs are not shown. nd: not detected in 1 or 2 Envs.